JOURNAL OF SPACECRAFT AND ROCKETS
Vol. 46, No. 3, May–June 2009

Kinetics and Thermophysical Properties of Polymer Nanocomposites for Solid Rocket Motor Insulation

David W. K. Ho,* Joseph H. Koo,† and Ofodike A. Ezekoye‡
University of Texas at Austin, Austin, Texas 78712-0292

DOI: 10.2514/1.39798

Thermal protection materials are required to protect structural components of space vehicles during the reentry stage, missile launching systems, and solid rocket motors. Novel materials based on nanotechnology creating nontraditional ablators are rapidly changing the technology base for thermal protection systems. In this study, different polymer nanocomposite compositions were created by melt-compounded montmorillonite nanoclays or carbon nanofibers in a neat thermoplastic polyurethane elastomer polymer using twin-screw extrusion. The kinetic and thermophysical properties that are required to analyze the ablation characteristics were measured for selective thermoplastic polyurethane materials. Properties of the nanomodified systems were then compared against those of the current state-of-the-art insulation material, Kevlar®-filled ethylene-propylene-diene monomer and the neat thermoplastic polyurethane elastomer, for the investigation of kinetic parameters using the isoconversion technique. Based on temperatures at peak weight-loss rate, Kevlar-filled ethylene-propylene-diene monomer outranked the proposed formulations at all heating rates. Recognizing that ablation performance is a complex function of kinetic and thermophysical/transport properties, a surrogate test for ablation performance was investigated. Samples of neat and nanomodified thermoplastic elastomer were run in an oxygen-consumption (cone) calorimeter. The peak heat release rates of the nanomodified samples were substantially less than that of the neat thermoplastic elastomer.

Nomenclature

A	=	preexponential factor
A_s	=	maximum mass loss attainable
Cpm	=	°C/ min
c_p	=	specific heat
$D_{0.1}$	=	dispersion parameter
d	=	characteristic length scale
E	=	activation energy
E_{avg}	=	average activation energy
k	=	thermal conductivity
n	=	order of reaction
R	=	universal gas constant
$\dot{s}$	=	recession rate
T	=	temperature
t	=	time
w	=	instantaneous weight
X_s	=	solid conversion
α	=	thermal diffusivity
β	=	heating rate
δ	=	thickness of pyrolysis zone
ρ	=	density
τ	=	characteristic time scale

Subscripts

diff	=	diffusion
f	=	final
max	=	maximum
o	=	initial

Received 16 July 2008; revision received 18 March 2009; accepted for publication 19 March 2009.

*Graduate Student, Department of Mechanical Engineering; currently Alliant Techsystems, Inc., Elkton, MD. Member AIAA.

†Senior Research Scientist and Director, Solid Freeform Fabrication Consortium, Department of Mechanical Engineering, 1 University Station, Mail Stop C2200; jkoo@mail.utexas.edu. Associate Fellow AIAA (Corresponding Author).

‡Professor, Department of Mechanical Engineering, 1 University Station, Mail Stop C2200.

I. Introduction

THERMOPLASTIC polyurethane elastomer nanocomposites (TPUNs) are a novel class of materials developed by the U.S. Air Force Research Laboratory (AFRL) that are lighter, exhibit better ablation performance and insulation characteristics, and possess a more cost-effective manufacturing process than the current baseline material, Kevlar®-filled ethylene-propylene-diene monomer (EPDM). In general, TPUN thermophysical and flammability properties are characterized using thermogravimetric analysis (TGA) for kinetic parameters, differential scanning calorimetry (DSC) for specific heat, laser flash for thermal diffusivity and thermal conductivity, dilatometry for coefficient of thermal expansion, cone calorimetry for heat release rates, smoke concentration, and gas generation, as well as other analytical techniques [1]. This paper will summarize the physical, thermophysical, and flammability properties and determination of the kinetic parameters of selective TPUNs with various nanoparticles and loadings. The intent is that the measured properties will be used in numerical modeling of the performance of these systems.

II. Background

A. Behavior of Thermal Protection Materials

Thermal protection materials are required to protect structural components of space vehicles during the reentry stage, missile launching systems, and solid rocket motors (SRMs). Polymeric composites have been used as ablative thermal protection systems for a variety of military and aerospace applications. Thermal protection materials such as carbon phenolics and carbon–carbon composites are used as spacecraft heat shields and as insulation and nozzle assembly materials for SRMs. These materials are exposed to thermochemical as well as particle impinging flow and are subjected to high temperatures in excess of 3000°C with very high heating rates for a short duration [2–4].

Thermochemical ablation refers to the phenomenon of surface recession of an ablative due to severe thermal attack by an external heat flux. The initial heat transfer in the ablative occurs by pure conduction, and the resulting temperature rise causes material expansion or shrinkage, which may be associated with pure thermal

expansion, moisture vaporization, pyrolysis, etc. When the material reaches a sufficiently high temperature, thermochemical degradation or pyrolysis of the polymer matrix begins. The pyrolysis reactions result in the production of decomposition gases and solid carbonaceous char residue. The thermal expansion and the disappearance of solid material due to the decomposition result in an increase in porosity and permeability of the polymeric material. Thus, pyrolysis gases begin to escape through the polymeric material. For the thermal protection to be effective, all of these pyrolysis reactions must be strongly endothermic. The gases that flow through the char structure remove energy by convection, thus attenuating the conduction of heat to the reaction zone [2–4]. The ablative material is subdivided into the four zones: char layer, reaction layer, virgin layer, and backup structure, and the phenomena in each zone are depicted in Fig. 1 using NASA Johnson Space Center charring ablation material model AESOP-STAB [5].

B. Polymer Nanocomposites Technology

The introduction of inorganic nanomaterials as additives into polymer systems has resulted in polymer nanostructured materials exhibiting multifunctional high-performance polymer characteristics beyond those that traditional polymer composites possess. Multifunctional features attributable to polymer nanocomposites consist of improved thermal and flame resistance, moisture resistance, decreased permeability, charge dissipation, chemical resistance, and electrical and thermal conductivity [6–9]. Through control or alteration of the additives at the nanoscale level, one is able to maximize property enhancement of selected polymer systems to meet or exceed the requirements of current military, aerospace, and commercial applications. Traditionally, the preparation of a blend or composite with multifunctionality requires a tradeoff between desired performance, mechanical properties, cost, and processibility. Polymer nanocomposite technology can provide additional properties not present in the neat resin, without sacrificing the inherent processibility and mechanical properties of the neat resin.

Military interest in the use of polymer nanocomposites for ablatives has grown steadily since Vaia et al. [10] examined the ablative performance of polycaprolactam (nylon 6) nanocomposites. At least an order-of-magnitude decrease in the mass loss (erosion) rate was measured for the nanocomposite relative to the neat polymer. Vaia et al. suggested that this decrease in the erosion rate was due to a relatively tough, inorganic char formed during the ablation of these nanocomposites. The change in erosion properties occurs for as little as the addition of 2 wt % (≈0.8 vol. %) exfoliated mica-type layered silicate. Vaia et al. stated that the presence of the char layers does not alter the first-order decomposition kinetics of the polymer matrix. Based on our extensive research in polymer nanocomposites [9], certain nanoparticles have significant effects on the kinetics of nylon polymers. Instead, the nanoscopic distribution of silicate layers appears to create a uniform char layer that enhances the ablative performance. The formation of this char is only minutely influenced by the type of organic modification on the silicate surface of specific interactions between the polymer and the aluminosilicate surface, such as end-tethering of a fraction of the polymer chains through ionic interaction to the layer surface.

Patton et al. [11] reported the ablation, mechanical, and thermal properties of vapor-grown carbon nanofiber (VGCF)/phenolic resin composites for potential usage in solid rocket motor nozzles. Composites specimens with varying loadings (30 to 50 wt %), including one sample with rayon carbon fiber plies, were prepared and exposed to a plasma torch for 20 s with a heat flux of 16.5 MW/m^2 at approximately 1650°C. Low erosion rates and little char formation were observed. When fiber loadings increased, mechanical and ablative properties improved. The VGCF composites had low thermal conductivities (approximately 0.56 $W/m \cdot K$), indicating that they are good insulating materials. Patton et al. surmised that if a 65% fiber loading in VGCF composite could be achieved, then ablative properties are projected to be comparable with or better than the composites currently used on the Space Shuttle reusable solid rocket motor. Note that low recession rates are not necessarily the only measure of performance for a sacrificial thermal protective system. Often a more important measure of performance is the thermal response of the bondline between the ablator and the protected structure.

Koo et al. [12,13] and Koo and Pilato [14] reported two new classes of polymer nanocomposites that are lighter and have better ablation performance and insulation characteristics than current state-of-the-art materials. For the rocket motor internal insulation [12], thermoplastic elastomers were selected as the base polymer incorporated with different amounts of montmorillonite (MMT) clay, VGCF, and polyhederal oligomeric silsesquioxane (POSS®).

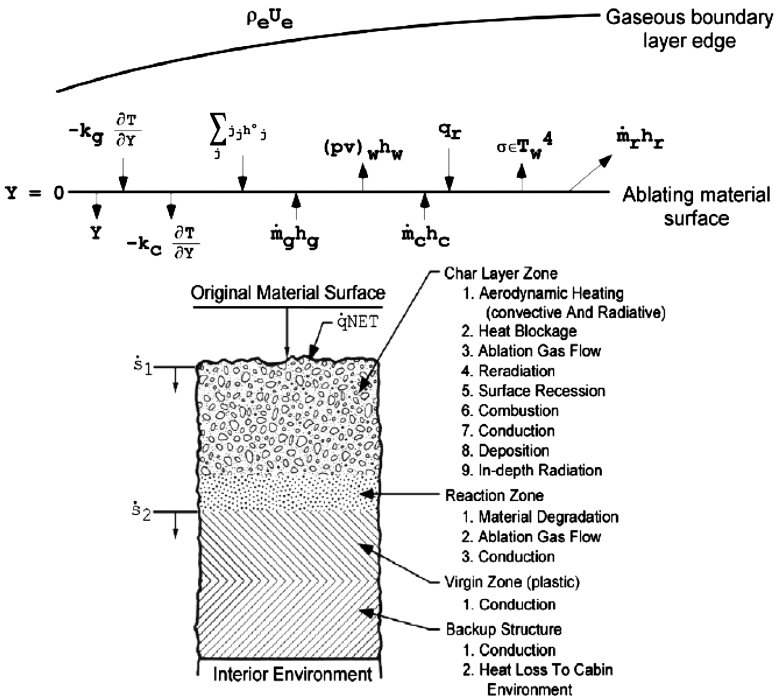

Fig. 1 Schematic diagram of NASA Johnson Space Center charring ablation material model AESOP-STAB.

Table 1 Results of quantitative measurements of TPU and TPUN-clay materials for polymer matrix 2102-90A

Loading level, wt %	Mean free-path spacing, μ, nm	Standard deviation, σ, nm	μ/σ	$D_{0.1}$, %	Classification
2.5	105.1	110.6	0.9503	8.4	Exfoliated
5.0	66.3	68.0	0.9750	8.6	Exfoliated
7.5	45.0	39.9	1.1278	9.8	Exfoliated
10.0	27.8	33.4	0.8323	7.5	Intercalated

Substantial performance improvement was observed with these thermoplastic elastomer nanocomposites as compared with industry-standard Kevlar-filled EPDM insulation material. For rocket nozzle ablative [13,14], MMT clay, VGCF, and POSS were incorporated into a resole phenolic and were impregnated into a rayon carbon fiber to fabricate into polymer matrix composites. Different loadings of MMT clay (2.5, 5, and 7.5 wt %), POSS (1, 3, and 5 wt %), and VGCF (20, 24, and 24 wt % without the rayon carbon fiber reinforcement) were incorporated into the phenolic resin. The simulated solid rocket motor (SSRM) was employed to test these nanocomposite rocket ablative materials (NRAMs) with an industry-standard ablative (MX-4926, a carbon phenolic composite) using a typical heat flux of 14 MW/m^2 with Al_2O_3 particle loading simulating particle impingement for a test duration of 15 s. The ablation rate of MX-4926 is about 0.4 mm/s. For the clay-NRAM group, only the 7.5 wt % clay-NRAM has a lower ablation rate than MX-4926. For the carbon nanofiber (CNF)-NRAM group, all three loadings have lower ablation rate than MX-4926, with 28% CNF-NRAM being the lowest. For the POSS-NRAM group, all three loadings have lower ablation rate than MX-4926, with 5 wt % POSS-NRAM being the lowest. All NRAMs have a lower maximum backside heat-soaked temperature than MX-4926. The CNF-NRAM group has the lower heat-soaked temperature, followed by the POSS-NRAM group, then the clay-NRAM group.

A recent review by Koo et al. [15] has shown continued progress in using polymer nanocomposites for rocket propulsion research. Polymer nanocomposites have been developed to enhance materials properties for high-temperature applications. The feasibility of using polymer nanocomposites is clearly demonstrated for rocket propulsion insulation, rocket nozzle ablative materials, carbon–carbon composites, and damage-tolerant high-performance epoxy fiber-reinforced composite systems. MMT clay, nanosilica, VGCF, and POSS can be easily incorporated into various polymers using high shear processing and appropriate manufacturing techniques to form nanocomposites. The level and uniformity of nanoparticles dispersion in the polymer matrix is essential to achieve the desired properties' enhancement.

Elastomeric materials are used as internal ablative and insulative materials for rocket motor casings. Kevlar-filled EPDM is the industry standard for this application. Because the elastic modulus of rubbers is low, they also act as absorbers during transportation and as insulators for extreme temperature changes during storage for the solid propellant. The temperature of the solid-propellant combustion products often reaches several thousands of degrees. Because of the very short duration of exposure to high temperature on the elastomeric materials, they are adequate as insulation materials for solid rocket motors [16,17]. Elastomers are linear polymers, though most of them form no solid carbonic residue under thermal decomposition and will form a melt film only in the presence of specific additives. Thus, fillers play an important role in providing the necessary erosion resistance, heat-shielding properties, and mechanical strength. The introduction of various fillers can change the physical, mechanical, rheological, and other properties of these elastomeric materials [18–20]. Engineered thermoplastic elastomer products such as Santoprene®, a thermoplastic rubber, are already demonstrating their performance capability to replace EPDM in automotive weatherseal applications [18]. An excellent cost/performance balance, a potential weight reduction, coloring options, and coextrusion with rigid thermoplastic materials are the key advantages versus classical EPDM thermoset rubber profile systems [19,20].

III. Description of Materials and Processing

A. Polymer System

Thermoplastic elastomer (TPE) is a family of rubberlike materials that can be processed and recycled like thermoplastics, unlike conventional vulcanized rubbers, which behave like thermosets. An example of a TPE is PELLETHANE™ 2102-90A.[§] PELLETHANE is a thermoplastic polyurethane elastomer (TPU) material, consisting of polyester polycaprolactam and manufactured by Dow Plastics.

B. Montmorillonite Nanoclays

MMT nanoclay is a widely investigated nanoparticle, most commonly formed by in situ alteration of volcanic ash. Its sheet structure consists of layers containing the tetrahedral silicate layer and the octahedral alumina layer. Each sheet of MMT nanoclay has a thickness of approximately 0.96 nm. MMT nanoclays are able to improve mechanical properties, barrier performance, and application processing when full exfoliation is achieved in a polymeric material. To achieve exfoliation in various continuous phases, surface treatment of the nanoclay is needed. The MMT nanoclay of choice in this project is Cloisite® 30B, which is a surface-treated montmorillonite manufactured by Southern Clay Products, Inc. [21].[¶] Cloisite additives allow complete dispersibility and miscibility with many different resin systems. Surface treatment is accomplished with ion exchange between inorganic alkali cations on the clay surface with the desired organic cation. In this case, quaternary ammonium ions are chosen, and they act as a compatibilizing agent between the interface of MMT nanoclay and the continuous phase of the TPU. A specific chemical pretreatment modifier (MT2EtOH: methyl, tallow, bis-2-hydroxyethyl, and quaternary ammonium) is used for the preparation of Cloisite 30B.

C. Carbon Nanofibers

CNFs are a form of vapor-grown carbon fiber, which is a discontinuous graphitic filament produced in the gas phase from the pyrolysis of hydrocarbons. CNFs are able to combine many of the advantages of these other forms of carbon for reinforcement in engineered polymers. CNFs also have transport and mechanical properties that approach the theoretical values of single crystal graphite but can be made in high volumes at low cost. The CNFs are manufactured by Applied Sciences, Inc., Pyrograf® Products by pyrolytic decomposition of methane in the presence of iron-based catalyst particles at temperatures above 900°C. CNFs are produced only in a discontinuous form, in which the length of the fiber can be varied from about 100 μm to several centimeters, and the diameter is on the order of 100 nm. The CNFs used in the study are PR-19-PS CNF [21,22]. The abbreviation PS denotes that the carbon nanofibers are pyrolytically stripped CNFs. PR-19-PS CNF has fiber diameters of 100 to 200 nm and fiber lengths of 30 to 100 μm.

D. Processing of Materials and Selection of Candidates

Twin-screw extrusion technique was used for blending the 2102-90A TPU with different loading levels of Cloisite 30B nanoclay (2.5, 5, 7.5, and 10 wt %) and PR-19-PS CNF (5, 10, 15, and 20 wt %). In

[§]Data available online at http://www.dow.com/PublishedLiterature/dh_0076/0901b80380076430.pdf?filepath=footwear/pdfs/noreg/306-00486.pdf&fromPage=GetDoc [retrieved 2009].

[¶]Data available online at http://www.scprod.com/product_bulletins/PB%20Cloisite%2030B.pdf [retrieved 2009].

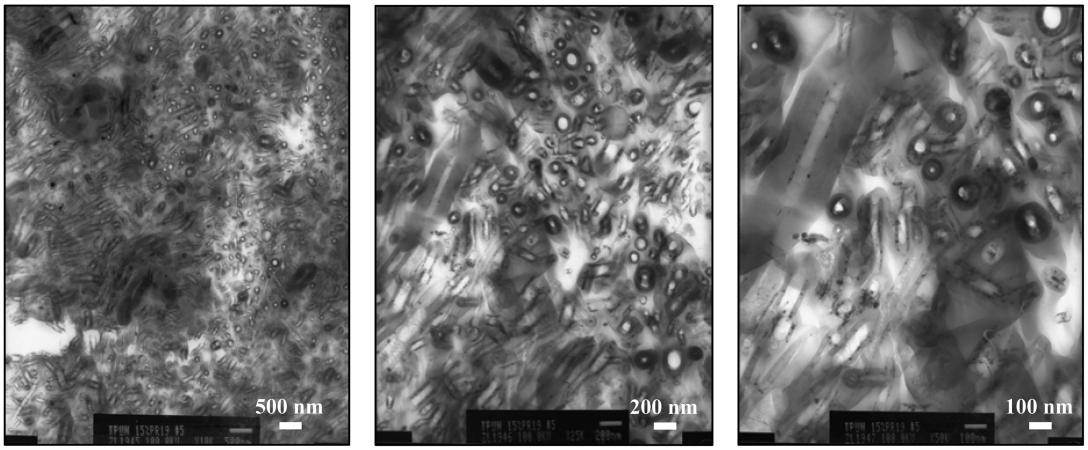

Fig. 2 Transmission electron micrographs of 15% PR-19-PS CNF in 2102-90A TPU in progressive magnifications.

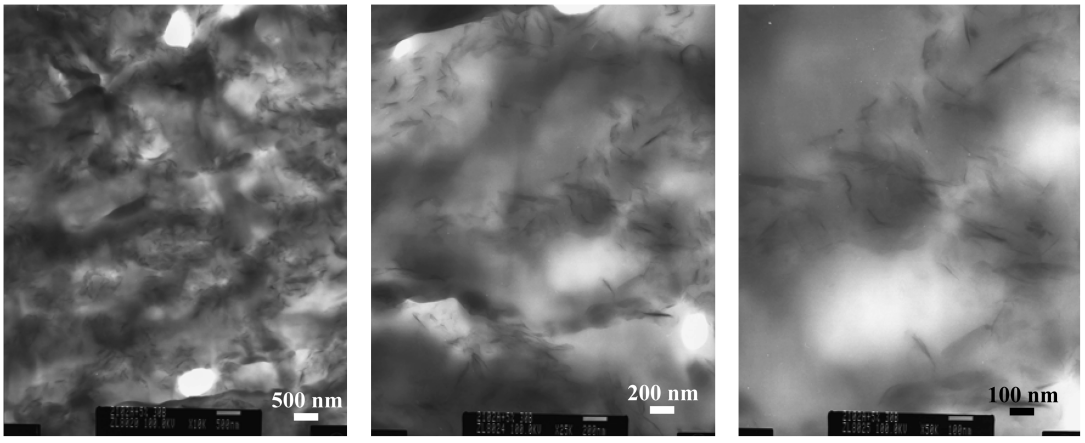

Fig. 3 Transmission electron micrographs of 5% Cloisite 30B nanoclay in 2102-90A TPU in progressive magnifications.

past work, selected TPU blends with the baseline Kevlar-filled EPDM were tested for ablation performance using the AFRL Pi-K char motor with aluminized propellants for ablation. The 5% Cloisite 30B TPUN and 15% PR-19-PS CNF TPUN were ranked highest in terms of ablation resistance and mechanical properties for their respective family of nanoparticles, thus chosen for more detailed thermophysical and kinetic properties characterization in this study.

Luo and Koo [23] developed a general method to quantify the dispersion of nanoparticles in polymer matrices using transmission electron microscopy (TEM) analyses. The dispersion quantity D is defined as the probability of inclusion particle free-path spacing falling into a certain range of the mean spacing μ, according to the particle-spacing data frequency distribution. Two quantities, $D_{0.1}$ and $D_{0.2}$, are proposed, which are the probabilities of the particle free-path spacing falling into the ranges of $\mu \pm 0.1\ \mu$ and $\pm 0.2\ \mu$, respectively. Both normal and lognormal distributions are discussed, and in both cases, the quantities $D_{0.1}$ and $D_{0.2}$ are specified as monotonically increasing functions of μ/σ, where μ and σ are the mean particle free-path spacing and standard deviation, respectively. The dispersion parameter $D_{0.1}$, based on the measurement of the free-path spacing distance between the single clay sheets [24], carbon nanofibers, and multiwall carbon nanotubes [25] from the TEM images, are presented by Luo and Koo [24,25]. This methodology was adapted in this study. Table 1 shows the quantitative measurements of TPUN-clay in clay loadings for 2.5, 5.0, 7.5, and 10 wt % [24]. The quantitative analyses show that the $D_{0.1}$ values of the 2.5, 5.0, 7.5, and 10.0 wt % materials are 8.4, 8.6, 9.8, and 7.5%, respectively. Only the 10.0 wt % TPUN-clay formulation is classified in the intercalated state, and the other TPUN-clay formulations are classified in the exfoliated state.

Transmission electron microscopy analyses were conducted on the 15% PR-19-PS TPUN based on the Luo and Koo [25] method show uniform dispersion of carbon nanofibers in 2102-90A, depicted in Fig. 2. In addition to TEM analyses (Fig. 3), the 5% Cloisite 30B TPUN was also analyzed using wide-angle x-ray diffraction (WAXD) for dispersion, no peaks were observed in WAXD. The WAXD and TEM analyses based on the Luo and Koo method confirmed that the 5% Cloisite 30B TPUN achieved exfoliation in the polymer matrix.

Table 2 Results of kinetic parameters from thermogravimetric analysis

w_f/w_0	Range of w/w_0	E_{avg}, kcal/g-mol	A, min^{-1}	n	w/w_0
		Henderson [27]			
0.66	0.73–0.99	52.11	4.07×10^{46}	55.40	≥ 0.94
0.66	0.73–0.99	52.11	7.77×10^{17}	3.81	<0.94
		Ho et al. [30]			
0.66	0.73–0.99	52.14 ± 6.15	4.10×10^{46}	55.36	≥ 0.94
0.66	0.73–0.99	52.14 ± 6.15	7.89×10^{17}	3.81	<0.94

IV. Experimental Approach

A. Thermogravimetric Analysis

The required data for calculating the kinetic parameters by TGA are temperature, weight loss, and the rate of weight loss. These data are obtained with a Perkin Elmer model TGA7 thermogravimetric analyzer. It has a vertical design with a high-sensitivity microbalance and electric platinum wound furnace, which is capable of heating rates up to 180°C/ min to a maximum temperature of 1000°C. The microbalance is located above the furnace and is thermally isolated from it. A hang-down wire is suspended from the balance down into the furnace. At the end of the hang-down wire is the platinum sample pan. The sample temperature is measured with a chromel-alumel thermocouple located inside the furnace. The purging gas flow rate is regulated by a mass flow controller and is kept at 20 ml/ min.

B. Kinetic Rate Calculation

The rate of decomposition of a material can be modeled by the kinetic rate equation:

$$-\frac{1}{w_0}\frac{dw}{dt} = Af\left(\frac{w}{w_0}\right)^n \exp\left(-\frac{E}{RT}\right) \tag{1}$$

where A is the preexponential factor, E is the activation energy, n is the order of reaction, and $f(w/w_0)$ is an arbitrary function of instantaneous weight fraction. To predict the thermal response of a material, accurate values of these kinetic parameters over the range of decomposition are required in a thermal model. In the literature, there are several methods to determine the kinetic parameters from experimental data. For degradation kinetics calculations, two

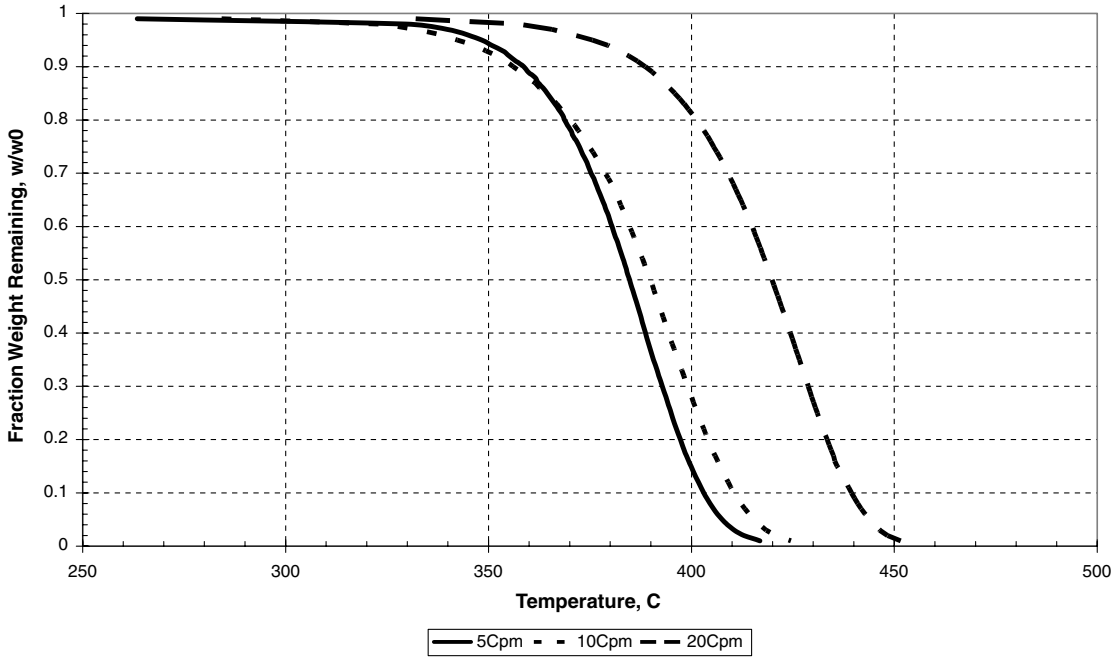

Fig. 4 Fraction of weight remaining for three heating rates for Plexiglas.

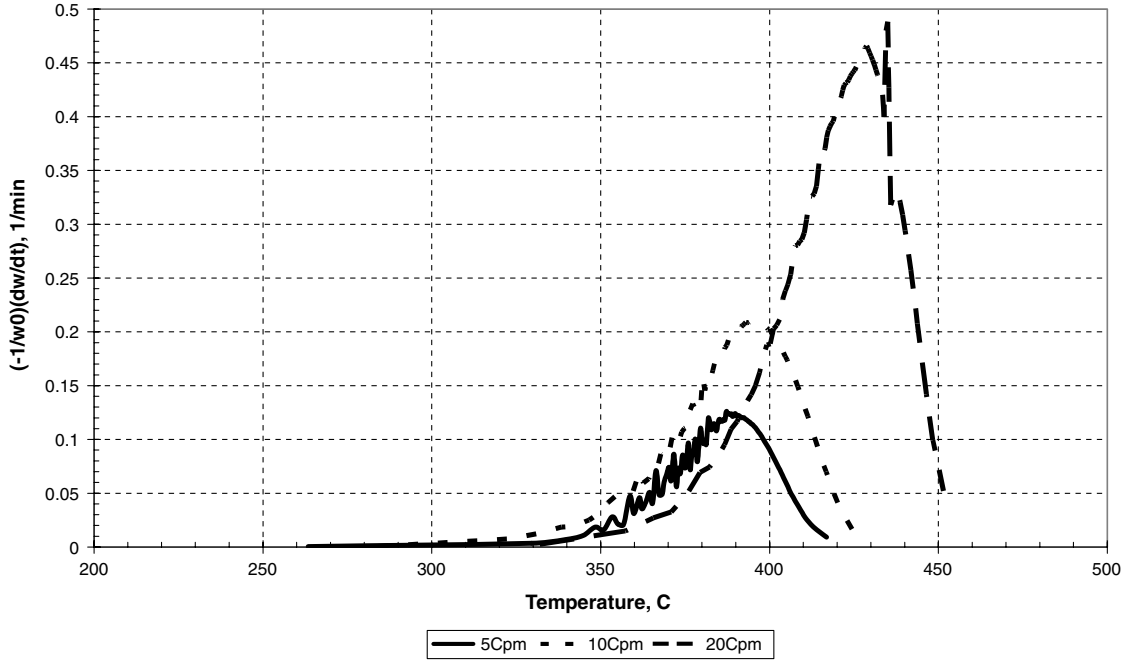

Fig. 5 Rate of weight loss for three heating rates for Plexiglas.

widely used methods, the modified Friedman method [26] used by Henderson [27] and the isoconversion method [28] based on the Ozawa–Flynn–Wall technique [29], will be briefly discussed, along with a benchmarking step (Sec. IV.C) to verify the methodology.

Henderson [27] proposed the modified Friedman method for calculating the kinetic parameters. Through mathematical manipulations of the Arrhenius kinetic rate equation (1), an average activation energy, preexponential factor, and order of reaction can be calculated based on TGA data linear curve fits at various heating rates. Another method that is widely used to describe kinetics is the isoconversion method [28]. This method assumes single-order reaction and the Ozawa–Flynn–Wall technique [29] in calculating activation energy and preexponential factor. These kinetic parameters imply that the thermal decomposition of the material can be expressed by a simple kinetic equation, with single effective values of A and E. By adjusting the order of reaction, a separate set of kinetic parameters can be obtained, but when plotting $\log A$ as a function of E, a linear curve fit can be observed using different values of n, which is a result of the kinetic compensation effect.

C. Benchmarking

Henderson [27] used the dynamic heating method to calculate the kinetic parameters for a variety of charring ablative composite materials. The authors established benchmarking progress on replicating the calculated kinetics by Henderson. The material of interest was chosen to be a rubber-modified glass phenolic composite, MXBE-350, fabricated by Fiberite Corporation (now known as Cytec Engineered Materials). This material was used extensively for high-temperature, high-heating-rate thermal protection applications such as the U.S. Navy vertical launching system. It consisted of 28% phenol-formaldehyde (phenolic)/14% acrylonitrile-butadiene resin

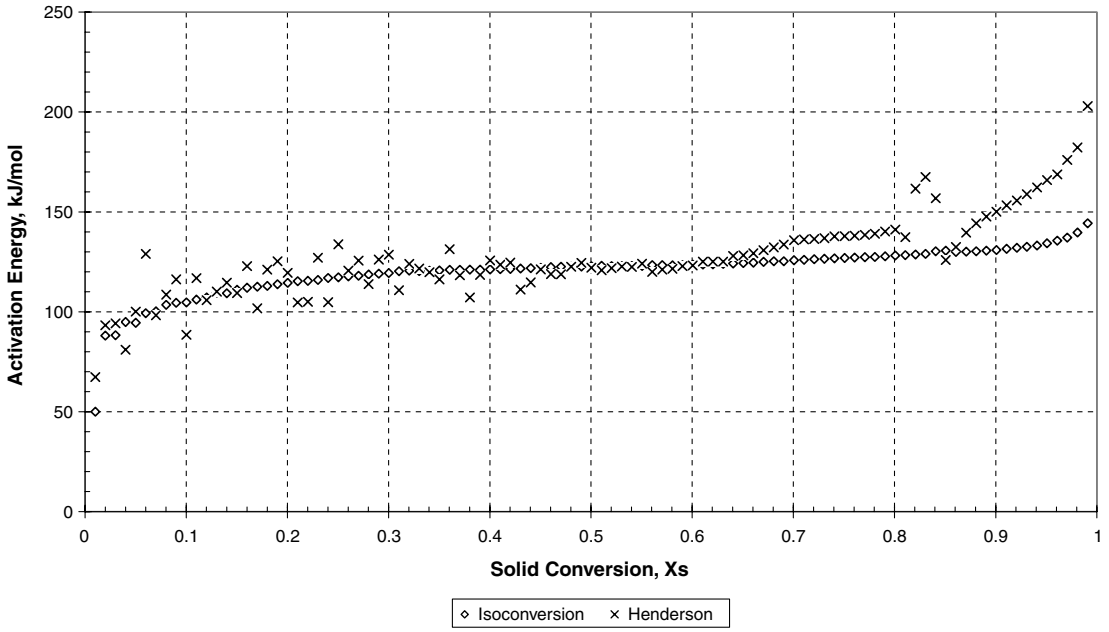

Fig. 6 Comparison of calculated activation energy of Plexiglas using isoconversion and Henderson methods.

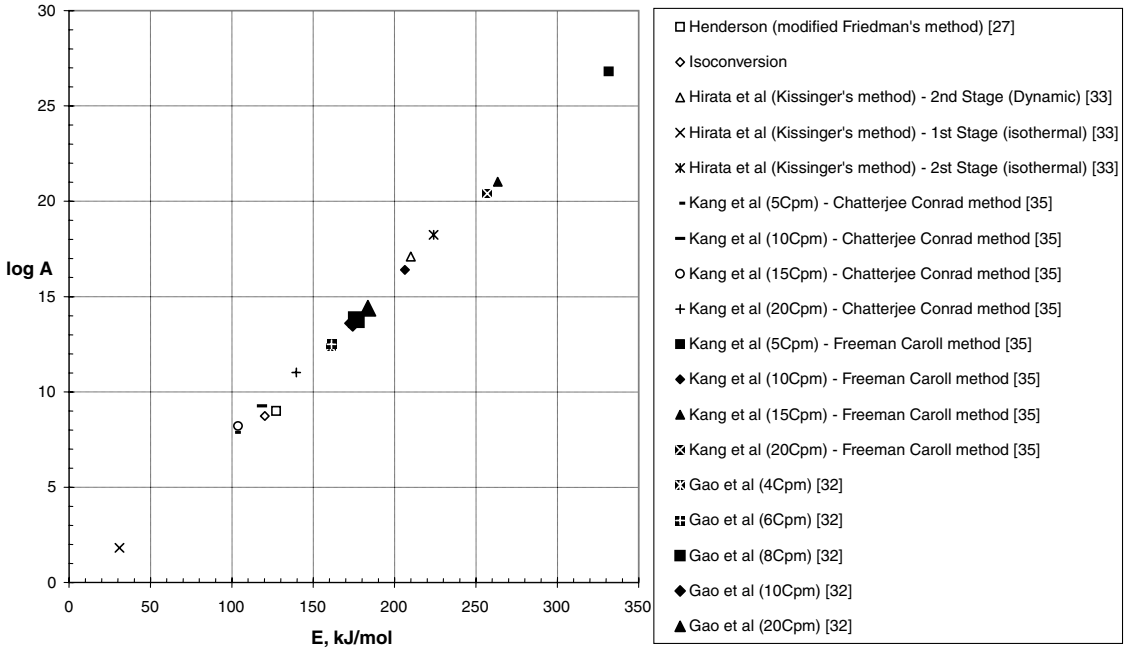

Fig. 7 Log (preexponential factor) vs activation energy of Plexiglas obtained by different authors and experimental conditions.

with 43% glass fiber (mat)/15% glass powder filler. The properties and modeling values for accurate modeling of the overall thermally induced response of the material were well characterized by Henderson.

Henderson [27] performed TGA in nitrogen at six different heating rates of 10, 20, 40, 80, 100, and 160°C/ min from room temperature to 950°C. Thermogravimetric data including the temperature, weight loss, and weight loss rate were tabulated up to the weight fraction remaining value of 0.73, and the final weight fraction remaining was 0.66. A plot of $\ell_n[(-1/w_0)(dw/dt)]$ as a function of $1/T$ yielded a linear fit for each value of weight loss. The slope of each linear curve fit would have a value of $-E/R$ and a y-intercept of $\ell_n[Af(w/w_0)]$. These values presented over the range from $0.73 \leq w/w_0 \leq 0.99$. The results of all the kinetic parameter calculations are summarized in Table 2.

To demonstrate bias, if any, between TGA instruments, a well-characterized material was chosen for a reference comparison in terms of replication of data. A vast amount of TGA data for common polymeric materials has been published in the open literature, including polymethyl methacrylate (PMMA or Plexiglas), polyvinyl chloride (PVC), polycarbonate (Lexan®), etc. By comparing TGA data obtained by the authors with those in the open literature, bias can be quantified into uncertainties for error analysis. PMMA was chosen to analyze for instruments bias and also kinetics calculation using both the Henderson and isoconversion methods. Experiments were conducted in nitrogen at three different heating rates (5, 10, and 20°C/ min) from room temperature to 900°C. Weight loss and weight-loss rates are shown in Figs. 4 and 5. Thermal degradation process occurs between 300 and 500°C. The average activation energy calculated using the Henderson and isoconversion methods are 127.2 and 120.3 kJ/mol, respectively, shown in Fig. 6, using the order of reaction of unity. The preexponential factor calculated using the Henderson and isoconversion methods are 1.00×10^9 and 5.34×10^8 min^{-1}, respectively.

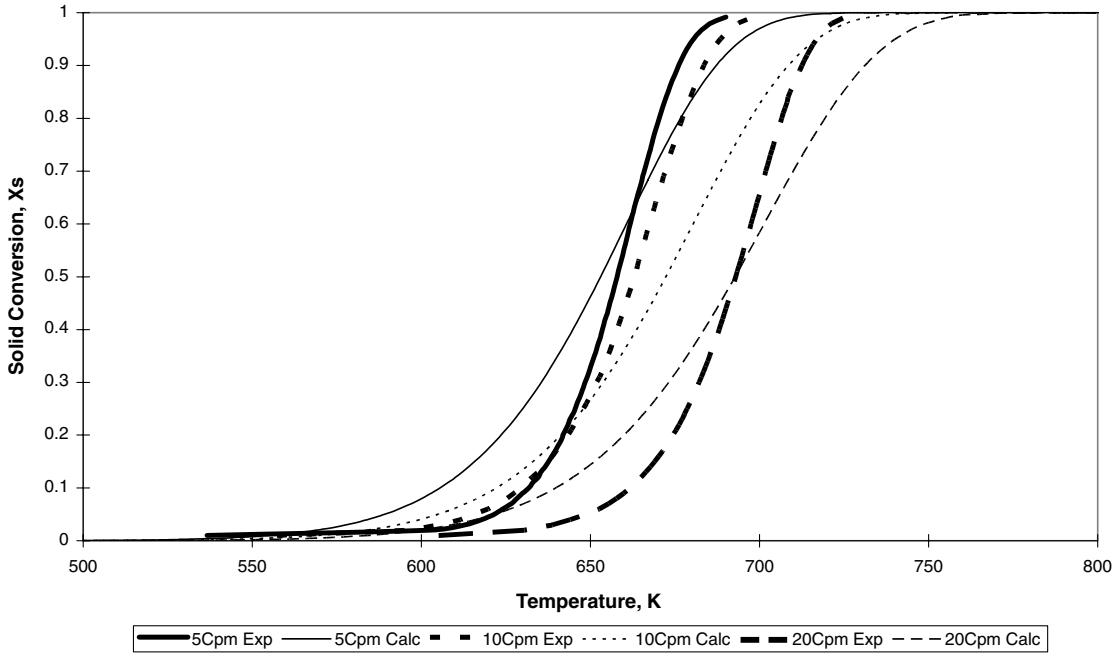

Fig. 8 Comparison of experimental and theoretical values of solid conversion vs temperature for different heating rates of Plexiglas.

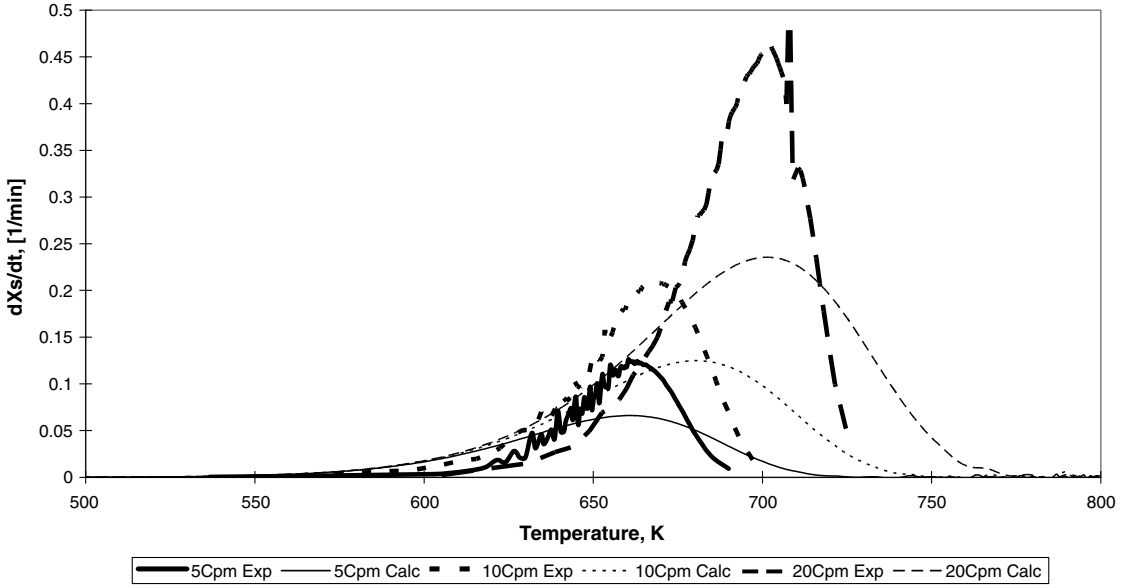

Fig. 9 Comparison of experimental and theoretical values of solid conversion vs temperature for different heating rates of Plexiglas.

These values have been compared with those obtained by other authors considering different operating conditions and calculation methods [31–36]. The values of $\log A$ and E are plotted in Fig. 7. Although the results shown have been obtained considering different values of reaction orders, an acceptable agreement is observed. This plot shows a linear relationship between $\log A$ and E. The kinetic compensation effect defines that if the apparent values of activation energy and preexponential factor are calculated using a single value on the order of reaction, their values would coincide on a linear fit of $\log A$ vs E with different values on the order of reaction. The results of solid conversion and rate of conversion calculated using the kinetic parameters by the isoconversion method have been compared with those found experimentally and are shown in Figs. 8 and 9, respectively, for the different heating rates. Some differences are clearly observed. The maximum values of dX_s/dt are lower than the experimental values, although they occur at about the same temperature, underestimating the weight-loss rates.

Closed-loop verification showed that both the modified Friedman and isoconversion methods provided reasonably accurate kinetic parameters for the benchmarking materials, but in the calculations for the proposed TPUN formulations, the modified Friedman method sometimes produced negative activation energy and an order of reaction that was clearly unrealistic. The isoconversion method did not encounter such problems, and it was adapted for the kinetics calculations in this study.

D. Using Low-Heating-Rate TGA Results to Applications Involving High Heating Rates

For the past 40 or more years, the applicability of using kinetics determined from low-heating-rate (5 to 20°C/ min) TGA experiments to applications in which local temperatures are changing at high heating rates (50 to 100°C/s) were unanswered. In this section, the authors will address the technical issues and provide a reasonable

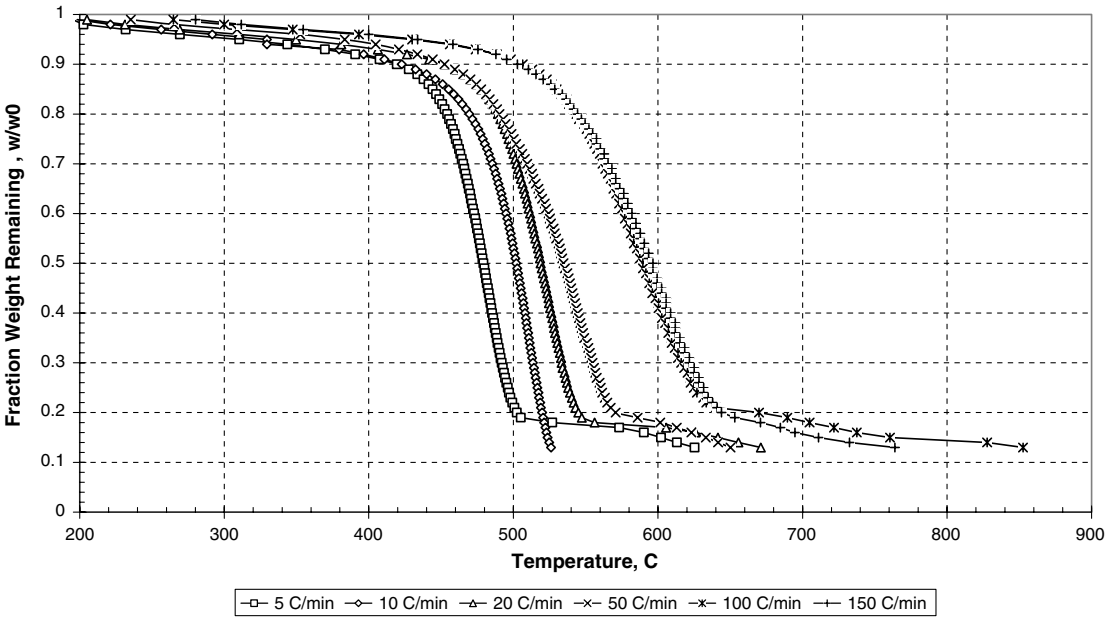

Fig. 10 Fraction of weight remaining for six heating rates for Kevlar-filled EPDM.

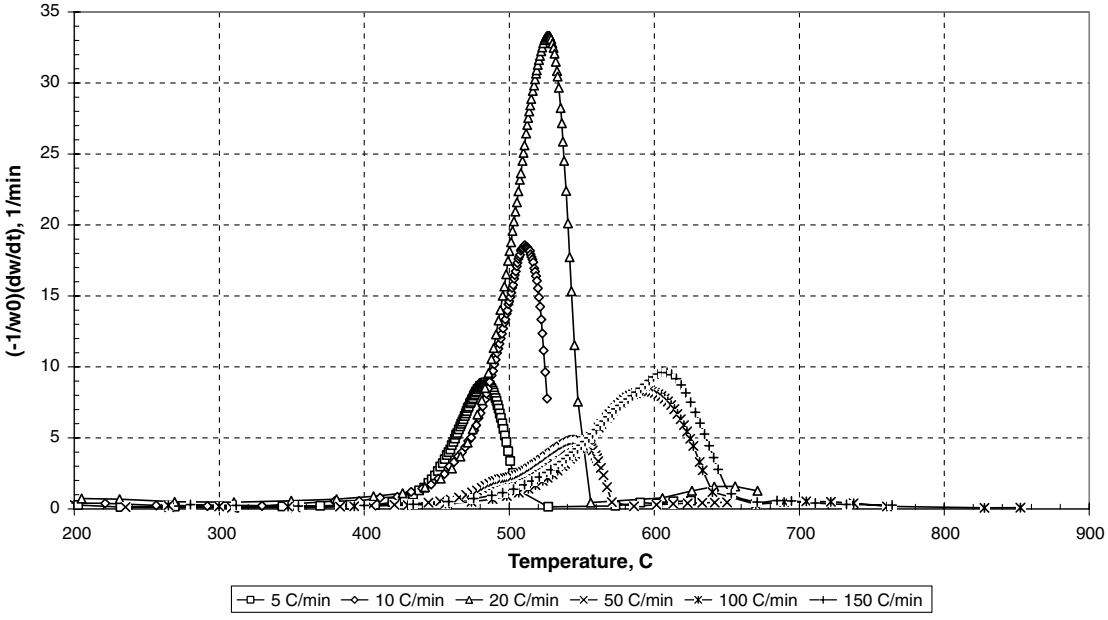

Fig. 11 Rate of weight loss for six heating rates for Kevlar-filled EPDM.

solution. Thermogravimetric analysis when combined with evolved gas analysis by Fourier transform infrared spectroscopy (FTIR) or mass spectrometry (MS) is often used to study thermal decomposition of polymers. Results are used to determine decomposition mechanisms and to develop rate expressions for different applications, including fire, solid rocket motor, and reentry vehicle. Although some current TGA instruments operate with controlled heating rates as high as 1000°C/ min, most experiments are done at much lower heating rates of about 5 to 50°C/ min to minimize temperature gradients in the specimen. The intended applications, such as solid rocket motor chamber, for rate expressions developed from TGA experiments often involve heating rates much higher than 50°C/ min. The heating rate can affect polymer decomposition by altering relative rates at which competing decomposition reactions occur. Erickson [37] analyzed the effect of heating rate on competing first-order decomposition reactions with Arrhenius rate constants and indicated that relative to heating rates of 5 to 50°C/ min, observable changes in decomposition behavior may occur when heating rates approach 1000°C/ min. Erickson's results [37] of PMMA specimens heated at 5 to 50°C/ min during TGA-FTIR experiments with specimens heated at rates on the order of 1000°C/ min during pyrolysis–gas-chromatography–FTIR experiments supported the analyses.

Erickson [37] concluded that when rate expressions are determined using TGA data obtained over a range of lower heating rates (1 to 50°C/ min) in which no significant variation in decomposition products is observed, it appears unlikely for values of E/R [where E is the activation for reaction rate (kW/mol) and R is the gas constant (kW/mol · K)] on the order of 15,000 K or greater that a potential competing reaction would significantly affect decomposition until

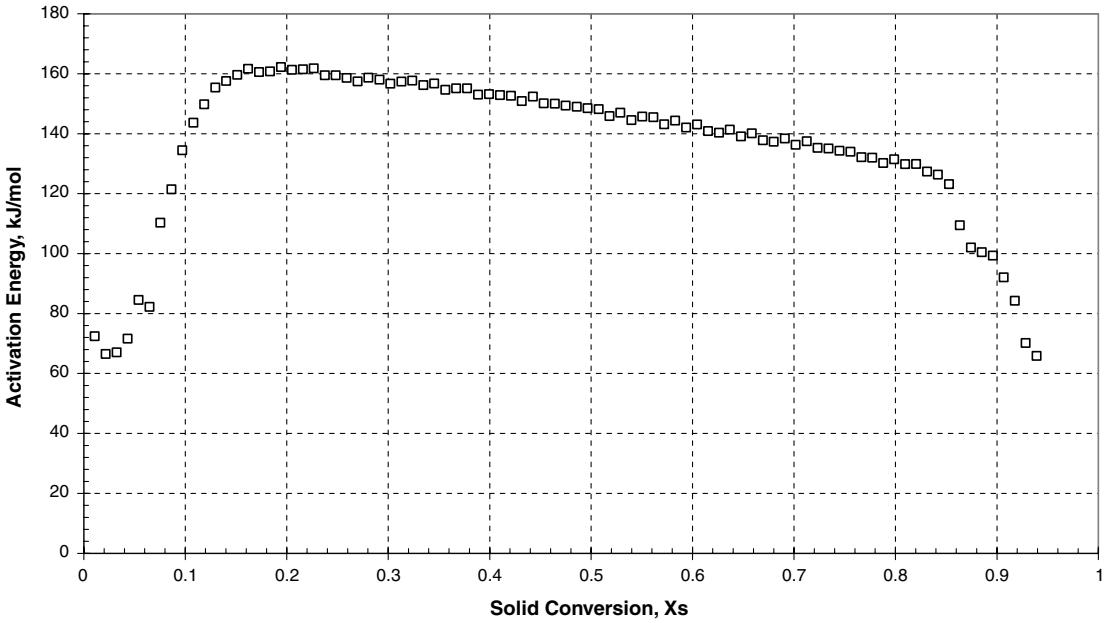

Fig. 12 Activation energy as a function of solid conversion of Kevlar-filled EPDM calculated by the isoconversion method.

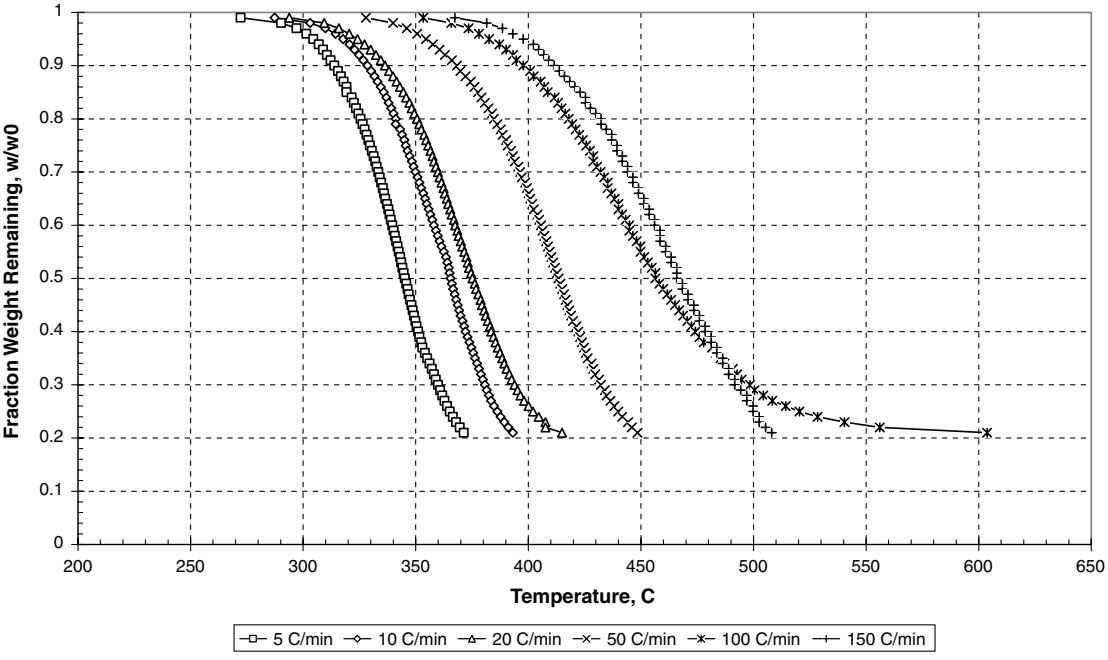

Fig. 13 Fraction of weight remaining for six heating rates for pure TPU.

heating rates are on the order of 1000°C/ min or greater. The rate expressions developed from the TGA experiments would appear to be applicable to fire-hazard analyses involving large-scale applications with heating rates to 1000°C/ min. These preliminary conclusions are supported by the experimental data from PMMA. The hypothetical reaction scheme considered was useful but simple. At low heating rates, most polymers decompose by mechanisms more complicated than simple depolymerization, and further analyses and experimental work should be done to more completely define conditions for applying low-heating-rate TGA results to fire-hazard analyses involving high heating rates.

Marschall and Oser [38] also reported simultaneous characterization of mass loss and pyrolysis gas species during ablator thermal decomposition. The authors couple a TGA to a versatile MS system via a heated quartz capillary line. The MS system contains both a quadrupole MS with an electron impact ionization source and a time-of-flight MS with a vacuum ultraviolet laser ionization source, enabling simultaneous measurement of the bulk gas composition and high-sensitivity detection and discrimination of hydrocarbon species. This combined TGA-MS apparatus has been demonstrated by investigating the thermal decomposition behavior of four different NASA-developed ablatives: PICA, PhenCarb-28, PhenCarb-20, and SRAM-20 [38].

The authors are currently conducting TGA experiments at high heating rates (up to 1000°C/ min) on several of our TPUNs to study the effect of heating rate and nanoparticle loading [39]. Advanced

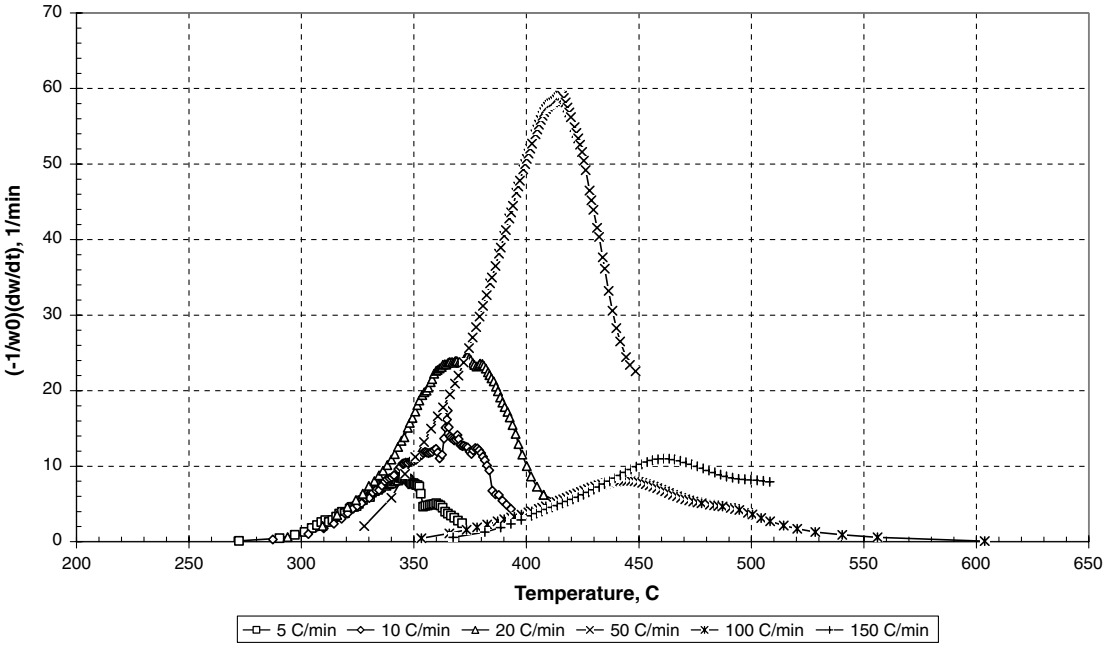

Fig. 14 Rate of weight loss for six heating rates for pure TPU.

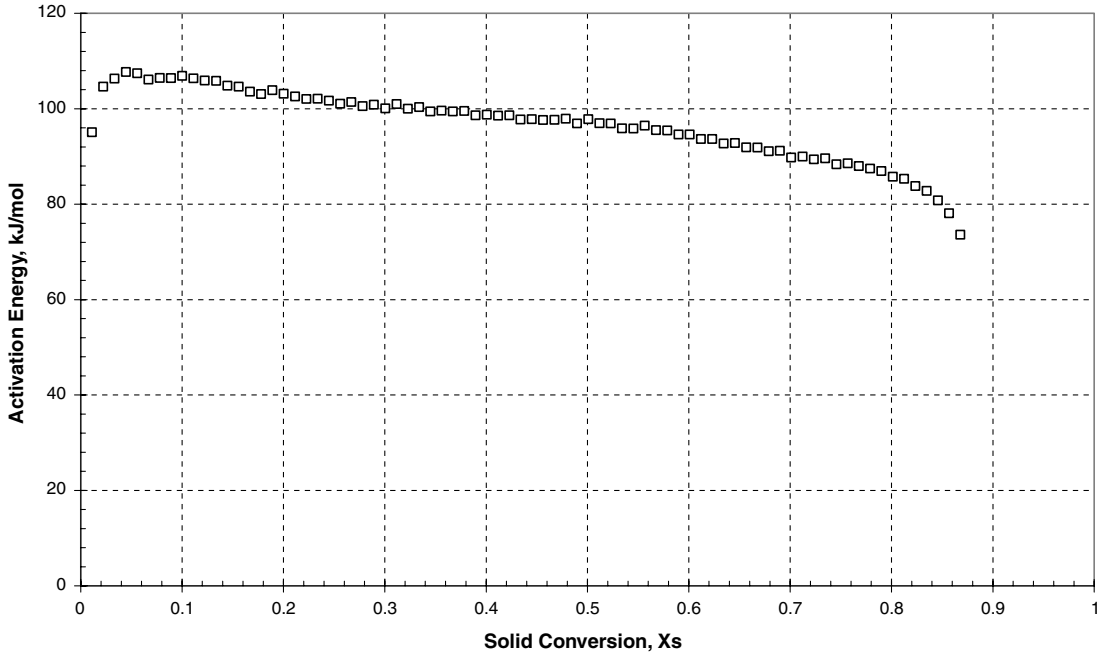

Fig. 15 Activation energy as a function of solid conversion of pure TPU calculated by the isoconversion method.

population-based models of thermoplastic degradation using optimization [40] with the TGA data will be employed to determine kinetic parameters [39].

E. Thermophysical and Flammability Properties Measurements

Thermophysical and flammability properties of TPU and TPUNs were evaluated. Density measurement was performed using a pycnometer. Specific heat capacity measurement was performed using DSC. Thermal diffusivity measurement was performed using the laser flash method. Thermal conductivity was calculated using data from density, specific heat capacity, and thermal diffusivity measurements. There is amazing similarity between how a sample ablates and its flammability properties. One measure of the ablative performance of a material is its ability to absorb heat when thermally assaulted. Often, a scenario-dependent parameter, the heat of ablation, is used to relate the incident heat flux to the mass flux of material leaving the ablator. A well-designed ablator will have a mass loss rate that is well tuned to the overall sample mass and to the heating environment. In flammability analysis, ASTM E1354 [41] (cone calorimeter) is used to measure the heat release rate of materials. Recognizing that the heat release rate is in fact proportional to the mass loss rate of volatiles liberated from the sample, one sees that inferences of the relative ability of samples to liberate volatiles can be made using cone calorimetry.

1. Density

The true volume of the material was measured using a pycnometer. By measuring the weight of the sample and employing Archimedes's principle of gas displacement and the technique of gas expansion, the density of the sample was obtained.

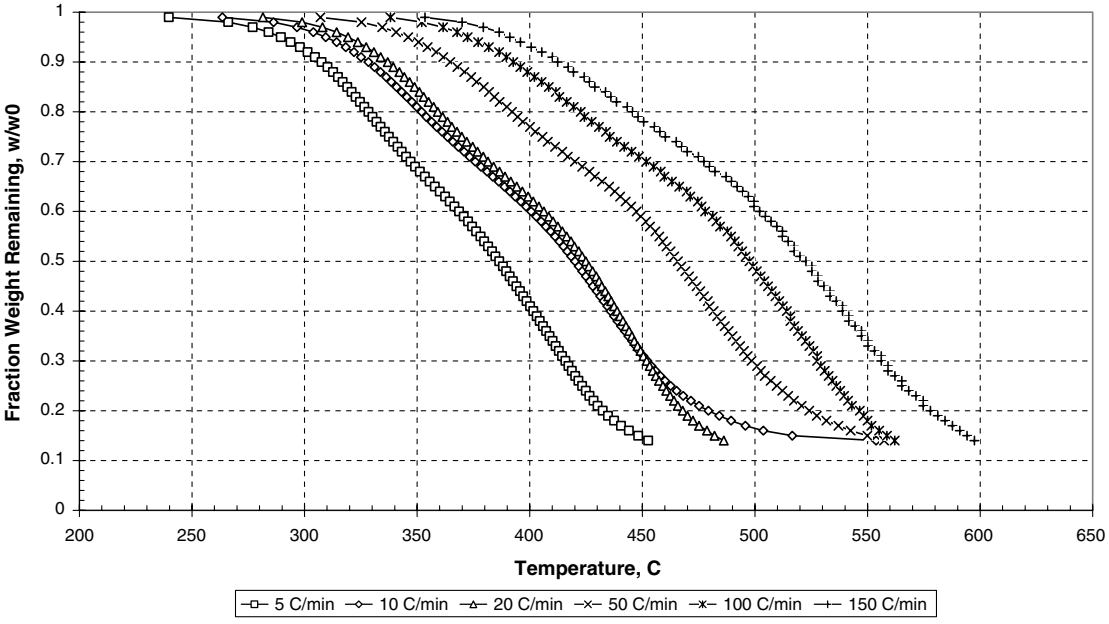

Fig. 16 Fraction of weight remaining for six heating rates for 5% Cloisite 30B TPUN.

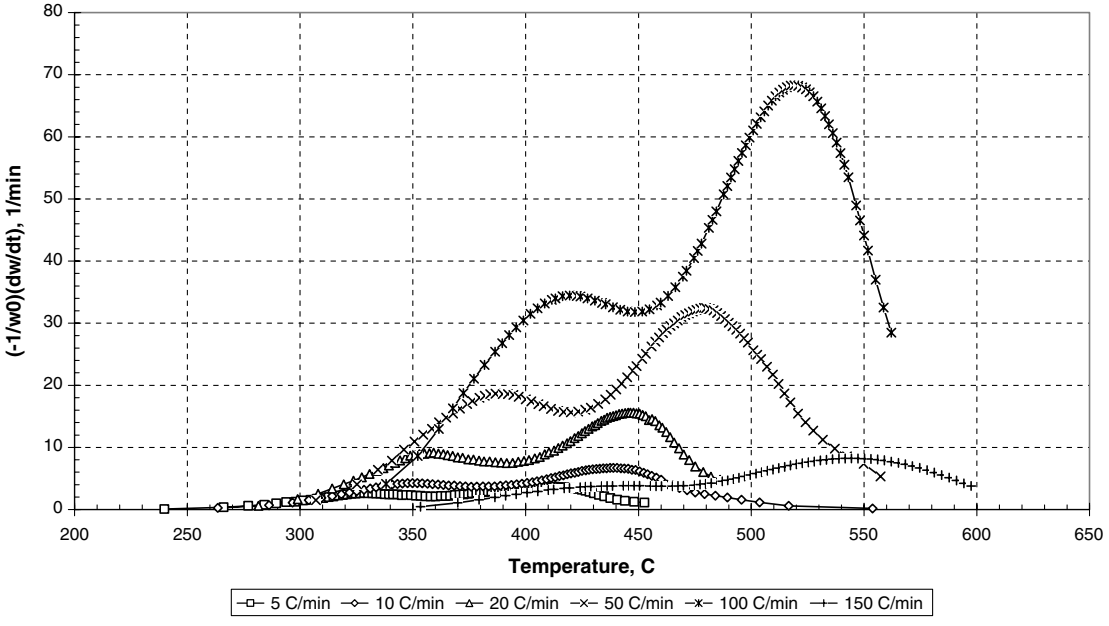

Fig. 17 Rate of weight loss for six heating rates for 5% Cloisite 30B TPUN.

2. Specific Heat

DSC was performed to obtain the specific heat of the TPU and TPUNs. A small amount of material sealed in a pan was heated at a set heating rate in a nitrogen-purging environment, and an analyzer recorded the heat flow needed to keep the temperature of the sample pan increasing at the same rate as the reference, or empty, pan. The specific heat was calculated by dividing the heat flow by the sample weight and the heating rate.

3. Thermal Diffusivity

Laser flash diffusivity at 45 and 55°C was performed to obtain the thermal diffusivity of the TPU and TPUNs. A laser is used to supply a high-intensity short-duration pulse of thermal energy to one face of a sample. The intensity of the beam was controlled by varying the laser power supply and use of attenuating filters. The resulting temperature rise of the other face of the sample was monitored using an infrared detector. Then the thermal diffusivity was determined from a numerical analysis of the infrared detector output.

4. Flammability Properties

As previously noted, both ablation- and fire-induced thermal degradation reveal similar aspects of a material's thermal degradation properties. Analysis of the degradation under firelike scenarios is useful in better understanding the material response for ablative applications. Additionally, the authors would like to identify dual usage of these novel materials for commercial markets. Because of these reasons, the flammability properties of TPU and TPUNs were also evaluated using the cone calorimeter per ASTM E1534 [41]. Average and peak heat release rates, mass loss, carbon monoxide (CO) emission, and smoke-concentration data were extracted from the experiments [42]. Cone calorimetry is based on the principle of oxygen-consumption calorimetry. A radiant

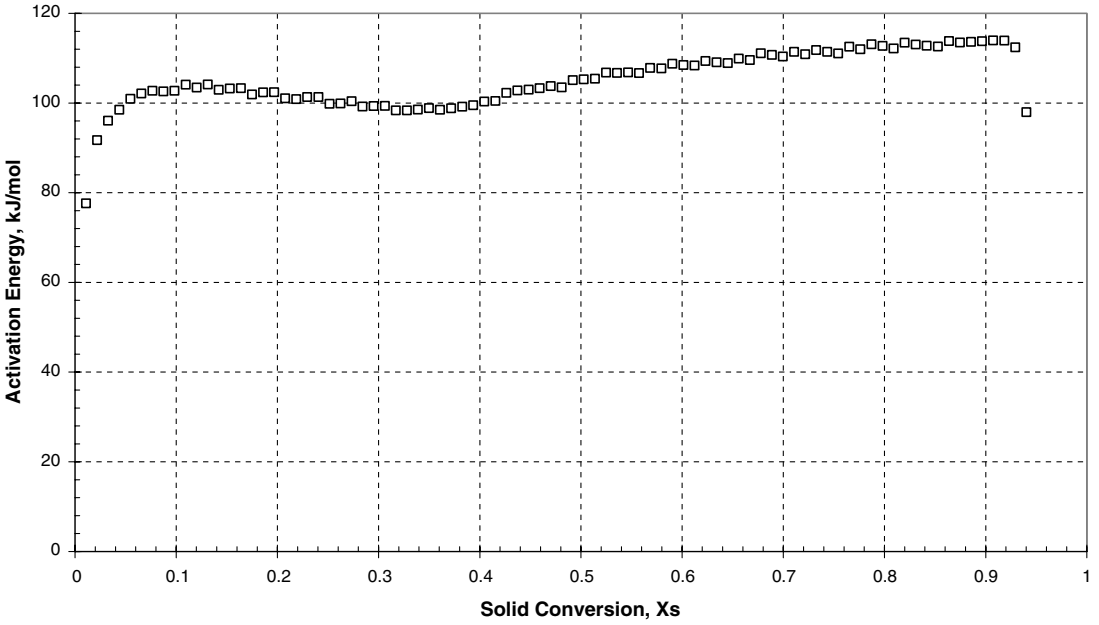

Fig. 18 Activation energy as a function of solid conversion of 5% Cloisite 30B TPUN calculated by the isoconversion method.

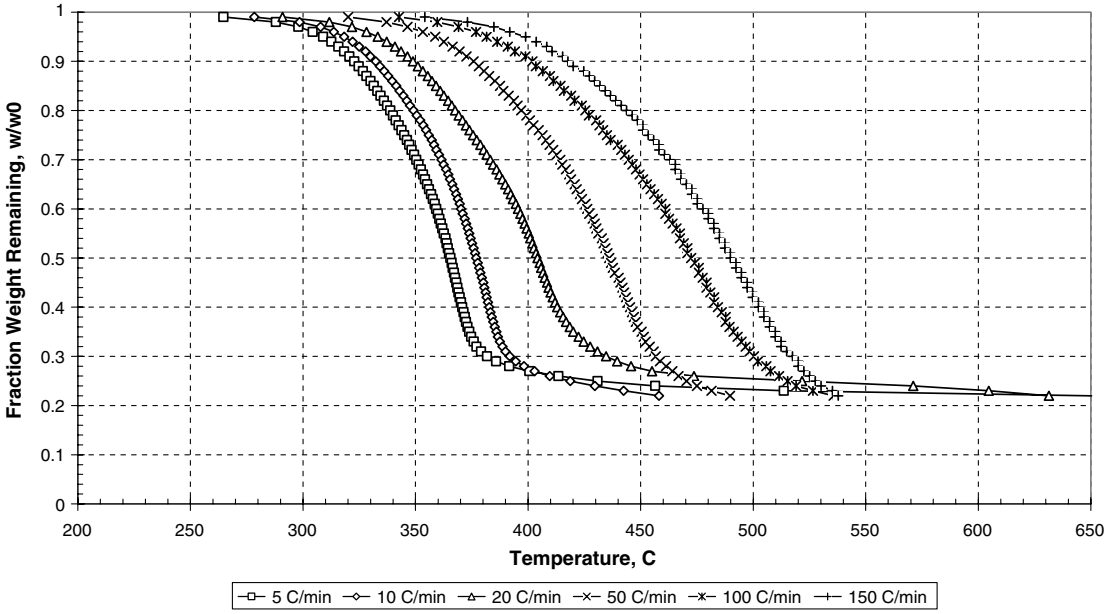

Fig. 19 Fraction of weight remaining for six heating rates for 15% PR-19-PS TPUN.

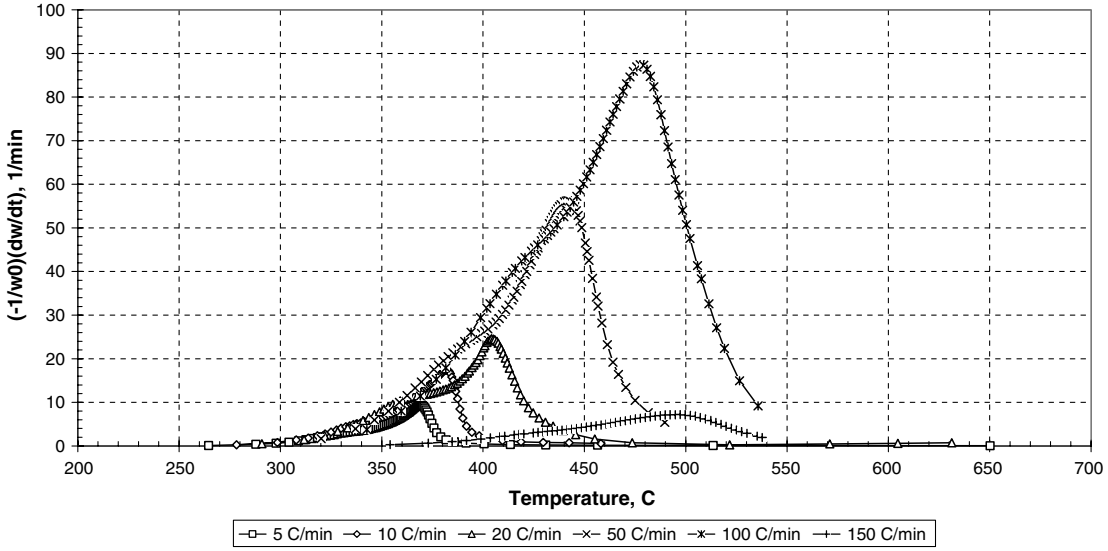

Fig. 20 Rate of weight loss for six heating rates for 15% PR-19-PS TPUN.

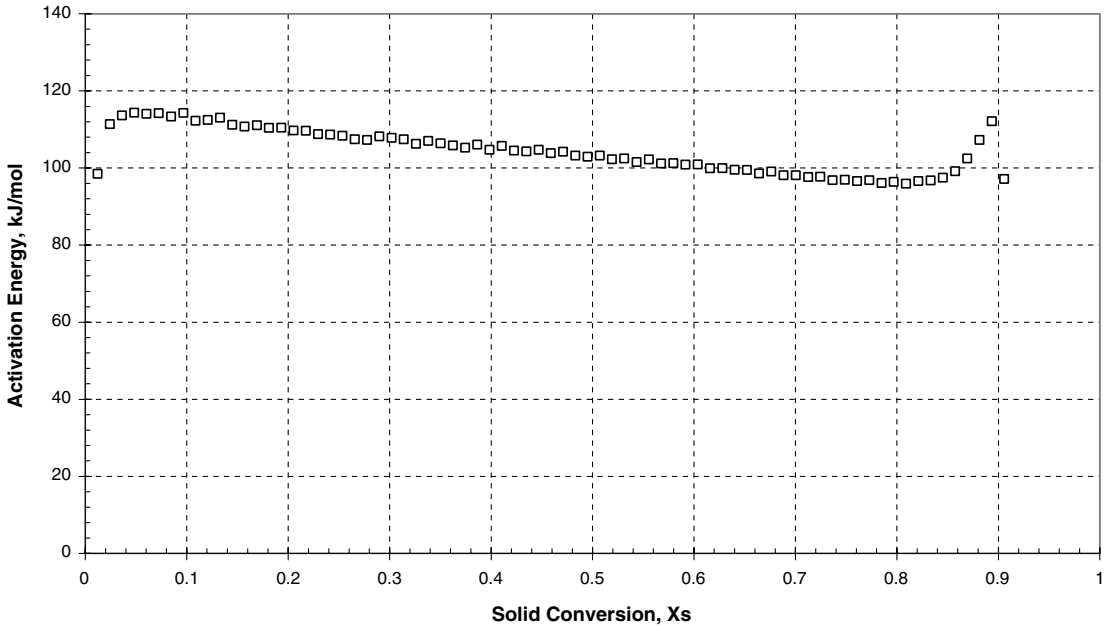

Fig. 21 Activation energy as a function of solid conversion of 15% PR-19-PS TPUN calculated by the isoconversion method.

electrical heater in the shape of a truncated cone irradiated a flat horizontal sample placed beneath it at a heat flux of 50 kW/m^2 in this study. The sample was placed on a load cell for continuous monitoring of its weight as it burned. The gas stream containing the combined combustion products was captured through an exhaust-duct system. Oxygen concentration in the exhaust stream was measured with an oxygen analyzer, and the heat release rate was determined by comparing the oxygen concentration with the value obtained without any sample. Carbon monoxide emission and smoke-concentration measurements were made in the exhaust duct by laser and detectors.

V. Discussion of Results

Thermogravimetric data of the materials are obtained at six different heating rates of 5, 10, 20, 50, 100, and 150°C/ min. Four formulations are tested in a nitrogen atmosphere: Kevlar-filled EPDM, pure TPU, 5% Cloisite 30B TPUN, and 15% PR-19-PS TPUN. Weight loss, rate of weight loss, and kinetic parameters using the isoconversion method for all four formulations are presented subsequently. Thermophysical properties including density, specific heat, thermal diffusivity, thermal conductivity, coefficient of thermal expansion of pure TPU, 5% Cloisite 30B TPUN, and 15% PR-19-PS TPUN are characterized.

A. Kinetic Parameters of Candidate Materials

1. Kevlar-Filled EPDM

The fraction of weight remaining (weight loss) and rate of weight loss versus temperature for Kevlar-filled EPDM are shown in

Table 3 Effective kinetic parameters results of thermogravimetric data

Material	E, kJ/mol	A, min^{-1}
Kevlar-filled EPDM	141.4 ± 16.6	4.50×10^{13}
Pure TPU	96.7 ± 7.9	4.29×10^{7}
5% Cloisite 30B TPUN	104.5 ± 7.7	3.80×10^{8}
15% PR-19-PS TPUN	104.4 ± 6.2	1.76×10^{8}

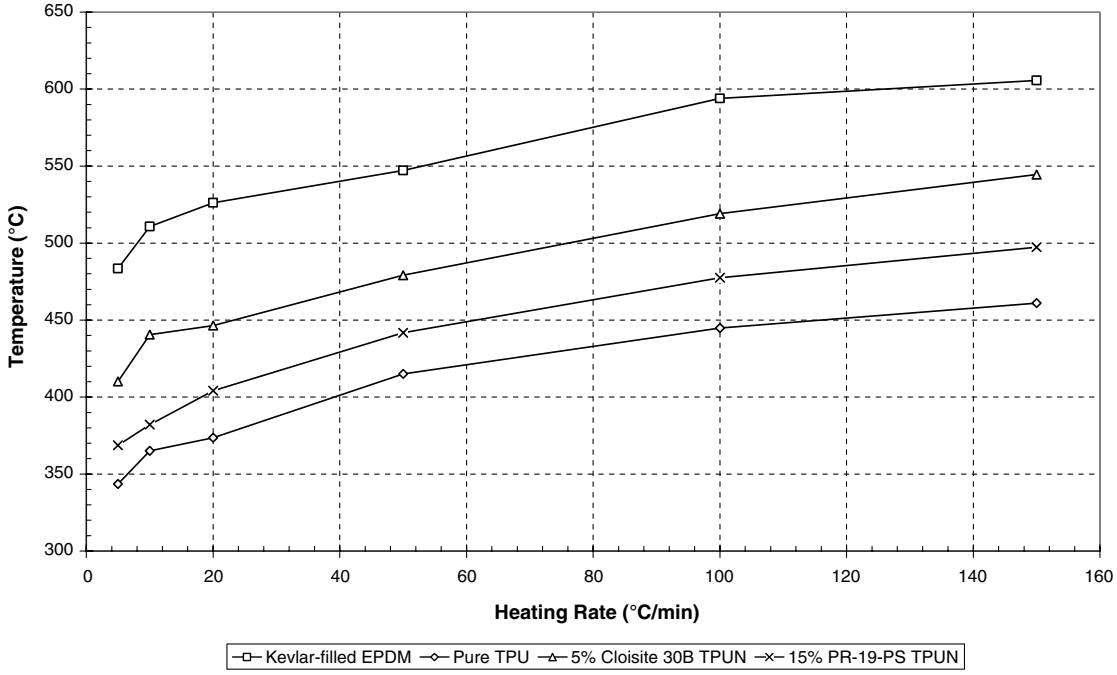

Fig. 22 Temperature of peak weight-loss rate as a function of heating rate for all formulations.

Figs. 10 and 11, respectively, for different heating rates. The fraction of weight remaining is plotted until 13% remaining mass, because no additional mass is lost as the temperature increases. As can be observed from the curve of weight loss, the onset temperature of decomposition shifts to higher temperatures with increasing heating rates. At the lowest heating rate of 5°C/ min, the onset temperature is approximately 430°C, whereas at the highest heating rate 150°C/ min, it is approximately 500°C. This is not a surprising result for this type of reaction. Note that when the reaction rate is in fact of Arrhenius form, then a Damköhler number (characteristic heating time divided by kinetic time) decreases with increasing heat rate. The effect of this is a relative slowing of the overall reaction progress, which results in a delay in the temperature and time at which the primary decomposition reaction takes place.

At a low heating rate (5°C/ min), the peak weight-loss rate occurs at a lower temperature, at approximately 484°C (757 K), and if the heating rate is 30 times larger (150°C/ min), the peak weight-loss rate occurs at approximately 612°C (885 K): a 16.9% increase. Thermal stability provides information about the degradation resistance of a material to thermal load. The activation energy calculated from the isoconversion method as a function of the solid conversion of Kevlar-filled EPDM is depicted in Fig. 12. Until a solid conversion of about 0.13, activation energy values are increasing with decreasing solid conversion, dictating the slow-weight-loss regime. When pyrolysis occurs, the activation energy reaches a peak value and slowly decays up to conversion of 0.90, and then it decreases further as it reaches complete conversion. The apparent average activation energy is 141.4 ± 16 kJ/mol, and the apparent preexponential factor is calculated to be 4.50×10^{13} min^{-1}.

2. Pure TPU

The fraction of weight remaining and rate of weight loss versus temperature for pure TPU are shown in Figs. 13 and 14, respectively, for different heating rates. The pyrolysis reaction initiates at approximately 300°C (573 K). At a low heating rate (5°C/ min), the peak weight-loss rate occurs at a lower temperature, at approximately 343°C (616 K), and if the heating rate is 30 times larger (150°C/ min), the peak weight-loss rate occurs at approximately 461°C (734 K): a 19.1% increase. The calculated activation energy by the isoconversion method as a function of solid conversion of pure TPU is depicted in Fig. 15. Unlike Kevlar-filled EPDM, pure TPU degrades at lower temperatures. The activation energy value peaks at a conversion of 0.04 at approximately 108 kJ/mol and decreases slowly. The apparent average activation energy is 96.74 ± 7.9 kJ/mol, and the apparent preexponential factor is calculated to be 4.29×10^{7} min^{-1}.

3. 5% Cloisite 30B TPUN

The fraction of weight remaining and rate of weight loss versus temperature for 5% Cloisite 30B TPUN are shown in Figs. 16 and 17, respectively, for different heating rates. From the weight-loss rate curves, two reactions are observed. Fully exfoliated nanoclay particles increase the decomposition temperature as well as the temperature of peak weight-loss rate. At a low heating rate (5°C/ min), the peak weight-loss rate occurs at approximately 410°C (683 K): a 10.9% increase in terms of thermal stability compared with pure TPU. When the heating rate is 30 times larger (150°C/ min), the peak weight-loss rate occurs at approximately 544°C (817 K): a 19.6% increase by heating rate and an 11.3% increase at the same heating

Table 4 Thermophysical properties of Kevlar-filled EPDM, TPU, and TPUNs

Material	Density, g/cm^3	Specific Heat, J/g · °C	Thermal Diffusivity, 10^{-7} m^2/s	Thermal Conductivity, W/m · °C
Kevlar-filled EPDM [44][a]	1.16	1.424	2.196	0.363
Pure TPU[b]	1.18	1.514/1.524	1.133/1.007	0.202/0.180
5% Closite 30B TPUN[b]	1.21	1.814/1.886	1.087/1.057	0.239/0.241
15% PR-19-PS TPUN[b]	1.27	1.473/1.491	1.583/1.523	0.296/0.288

[a]Kevlar-filled EPDM values were measured at room temperature.
[b]TPU and TPUN values were measured at 45 and 55°C.

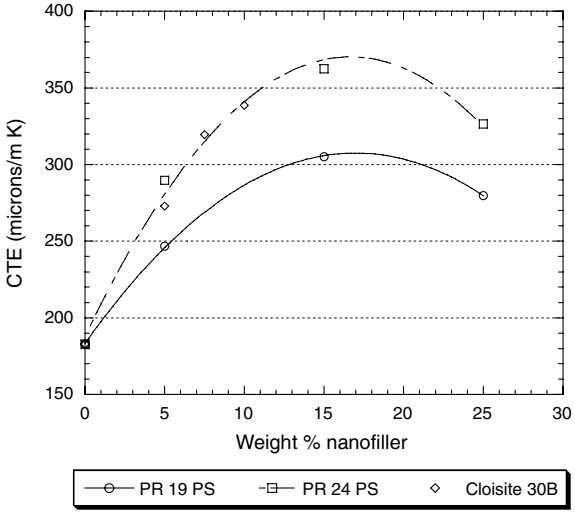

Fig. 23 Coefficient of thermal expansion of neat TPU and TPUNs.

rate compared with pure TPU. The activation energy calculated by the isoconversion method as a function of solid conversion of 5% Cloisite 30B TPUN is depicted in Fig. 18. Unlike Kevlar-filled EPDM and pure TPU, the activation energy follows two regimes because two reactions occur. The activation energy required to complete the first reaction has an average value of 99.9 kJ/mol. From a solid conversion of 0.37 onward, the activation energy steadily increases and peaks near complete conversion. Over this second region, the apparent average activation energy is 104.5 ± 7.7 kJ/mol, and the apparent preexponential factor is calculated to be 3.80×10^8 min^{-1}.

4. 15% PR-19-PS TPUN

The fraction of weight remaining and rate of weight loss versus temperature are shown in Figs. 19 and 20, respectively, for different heating rates. There is a single reaction for the 15% PR-19-PS TPUN. Well-dispersed carbon nanofibers in the TPU resin also increase the decomposition temperature as well as the temperature of peak weight-loss rate. At a low heating rate (5°C/ min), the peak weight-loss rate occurs at approximately 368°C (641 K): a 4.1% increase in terms of thermal stability compared with pure TPU. When the heating rate is 30 times larger (150°C/ min), the peak weight-loss rate occurs at approximately 497°C (770 K): a 20.1% increase by heating rate and a 4.9% increase at the same heating rate compared with pure TPU. The activation energy calculated by the isoconversion method as a function of solid conversion of 15% PR-19-PS TPUN is depicted in Fig. 21. The apparent average activation energy is 104.4 ± 6.2 kJ/mol, and the apparent preexponential factor is calculated to be 1.76×10^8 min^{-1}. The results of all calculations are summarized in Table 3.

Chipara et al. [43] studied the thermal degradation of isotactic polypropylene (IPP) with various loadings (0, 1, 2.5, 5, 7.5, 10, 15, and 20 wt %) of carbon nanofiber composites in nitrogen. The inflection temperature of these IPP-CNF composites increases as the concentration of CNFs is increased. Thermogravimetric analysis data indicate the formation of a polymer carbon nanofiber interface. Based on TGA data, a two-layer structure is proposed for the CNF-IPP interface. The external layer is soft and has a thickness of about 10^2 nm that confines most polymer molecules in interaction with CNFs. The core layer is rigid and has a thickness on the order of a few nanometers. The excellent dispersion of CNFs within the polymeric matrix (IPP), confirmed by TEM data, supports the proposed interpretation.

Based on temperatures at peak weight-loss rates, Kevlar-filled EPDM outranked the proposed formulations at all heating rates, shown in Fig. 22. This observation contradicts the SRM ablation experiments performed earlier. However, the percentage of temperature increases of peak weight-loss rate from low heating rate (5°C/ min) to high heating rate (150°C/ min) or the thermal stability from 5 to 150°C/ min showed that the proposed formulations were better more stable than the neat formulation (19.6% for 5% Cloisite 30B TPUN and 20.1% for 15% PR-19-PS TPUN, but only 16.9% for Kevlar-filled EPDM). This trend falls in line with our SRM ablation data, which makes us wonder if it is valid to use low-heating-rate data for applications involving high heating rate. Further studies are in progress to address this issue [39].

The validity of extrapolation of heating rates in TGA experiments to heating rates in actual ablation conditions is frequently questioned. We can estimate the heating rate in a typical ablator by noting that the maximum temperature difference $\Delta T_{\max}$ in a steady-state ablation process is on the order of 3000°C, the recession rate $\dot{s}$ is approximately 0.1 mm/s, and the thickness of the pyrolysis zone can be estimated as $\delta \approx \alpha/\dot{s}$. Thus, the scaling for the temperature-rise rate is $\dot{s}^2 \Delta T_{\max}/\alpha$. For a nominal case for which the thermal diffusivity α is 0.1×10^{-6} m^2/s, we see that the temperature-rise rate is 300°C/s (18, 000°C/ min), which is approximately 120 times larger than our fastest heating rates. The rate of heating is a practical limitation on the use of TGA for ablation-property characterization.

Using similar scaling ideas, we discuss the validity of the isothermal specimen assumption for TGA samples as a function of heating rate. Assuming a sample characteristic length scale of d that is on the order of 1 mm for TGA samples, the time scale for diffusion over that length is $\tau_{\text{diff}} \sim d^2/\alpha$. The TGA heating rate in degrees per second is β. The product of the heating rate and characteristic diffusion time $\beta d^2/\alpha$ represents the characteristic temperature difference across the sample. The highest heating rate that we use is 150°C/ min (2.5°C/s). The characteristic temperature difference across the sample is thus approximately 25°C. Although this seems to be a large temperature difference, recognize that typical temperatures for degradation are approximately 400°C (673 K). As such, the relative temperature error, based on absolute temperatures, is less than 4% at the highest heating rates that we use.

B. Thermophysical and Flammability Properties

1. Thermophysical Properties

Thermal conductivity was derived based on the relationship $k = \alpha(T)\rho(T)c_p(T)$, where k is thermal conductivity, α is thermal diffusivity, ρ is density, and c_p is specific heat. All thermophysical properties data of Kevlar-filled EPDM [44], TPU, and TPUNs were tabulated in Table 4. As expected, both the 5% Cloisite 30B TPUN (TPUN-clay) and 15% PR-19-PS TPUN (TPUN-CNF) have higher densities than the neat TPU and Kevlar-filled EPDM materials. The specific heat of the TPUN-clay is substantially higher than the neat TPU and Kevlar-filled EPDM, whereas the TPUN-CNF is lower than the neat TPU. The thermal conductivity values of both the TPUN-clay and TPUN-CNF are higher than the neat TPU, with the carbon-based TPUN-CNF substantially more thermally conductive than the neat TPU. The thermal conductivity of Kevlar-filled EPDM (at room

Table 5 Summary of cone calorimetry data at irradiance heat flux of 50 kW/m^2

Material	Time to sustained ignition t_{ig}, s	PHRR, kW/m^2	Avg HRR 60 s after ignition, kW/m^2	Avg HRR 180 s after ignition, kW/m^2	Avg effective heat of combustion H_c, MJ/kg	Avg specific extinction area, m^2/kg
Pure TPU	32	2290	406	653	30	237
5% Closite 30B TPUN	34	664 (71% reduction)	560	562	25	303
5% PR-19-PS TPUN	27	624 (73% reduction)	532	456	22	295

temperature) is higher than the TPUN-CNF material (at elevated temperatures). The coefficient of thermal expansion (CTE) of the pure TPU, TPU-clay (Cloisite 30B) of various loadings, and TPU-CNF (PR-19-PS and PR-24-PS) of various loadings are shown in Fig. 23. All TPUNs have higher CTE than the pure TPU. The TPU-clay (Cloisite 30B) and TPU-PR-19-PS CNF have similar CTE, whereas the TPU-PR-24-PS CNF has lower CTE. All of these thermophysical properties need to be characterized in the charred state at elevated temperatures. Using relatively simple ideas, it would not be apparent that the changes in the thermophysical properties would positively impact the ablative performance of the samples.

2. Flammability Studies

In this study, 5% PR-19-PS TPUN instead of 15% PR-19-PS TPUN was tested under a radiant heat flux of 50 kW/m^2. Two samples of each formulation were tested for repeatability. The TPUNs were compared with the pure TPU. Average flammability properties were summarized in Table 5.

From the flammability data, the 5% Cloisite 30B TPUN showed a slightly increased time to sustained ignition (34 s) relative to the baseline TPU (32 s). The 5% PR-19-PS TPUN had a slightly lower time to ignition relative to the TPU. The 5% PR-19-PS TPU and the 5% Cloisite 30B TPU materials had significantly different peak heat

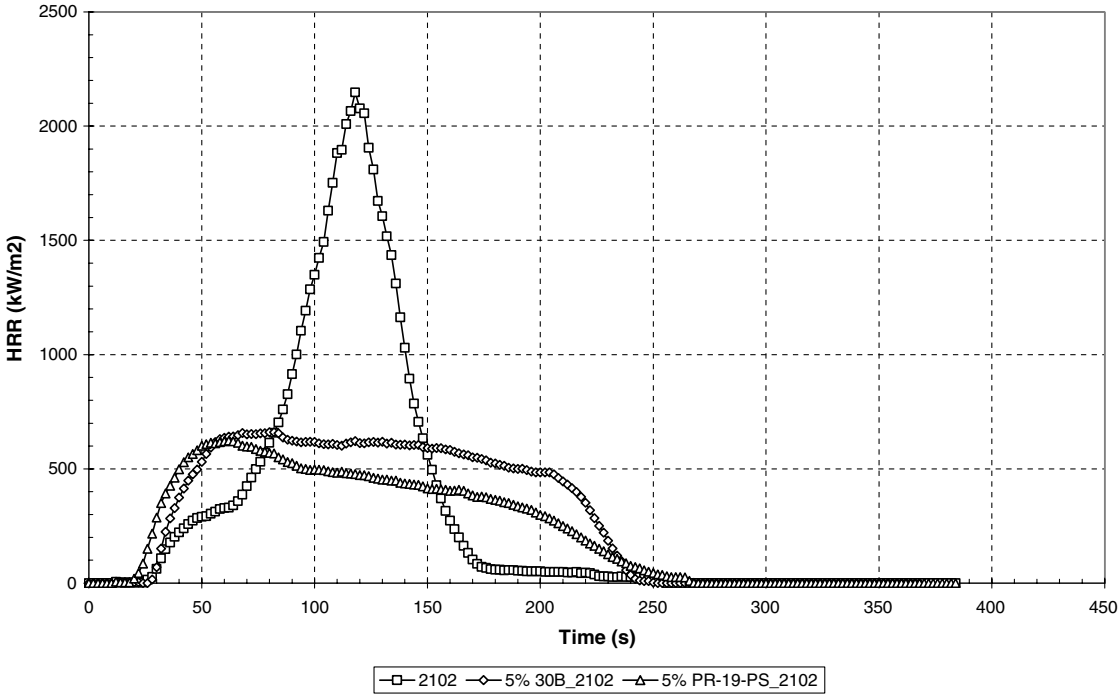

Fig. 24 Heat release rate of neat TPU and TPUNs.

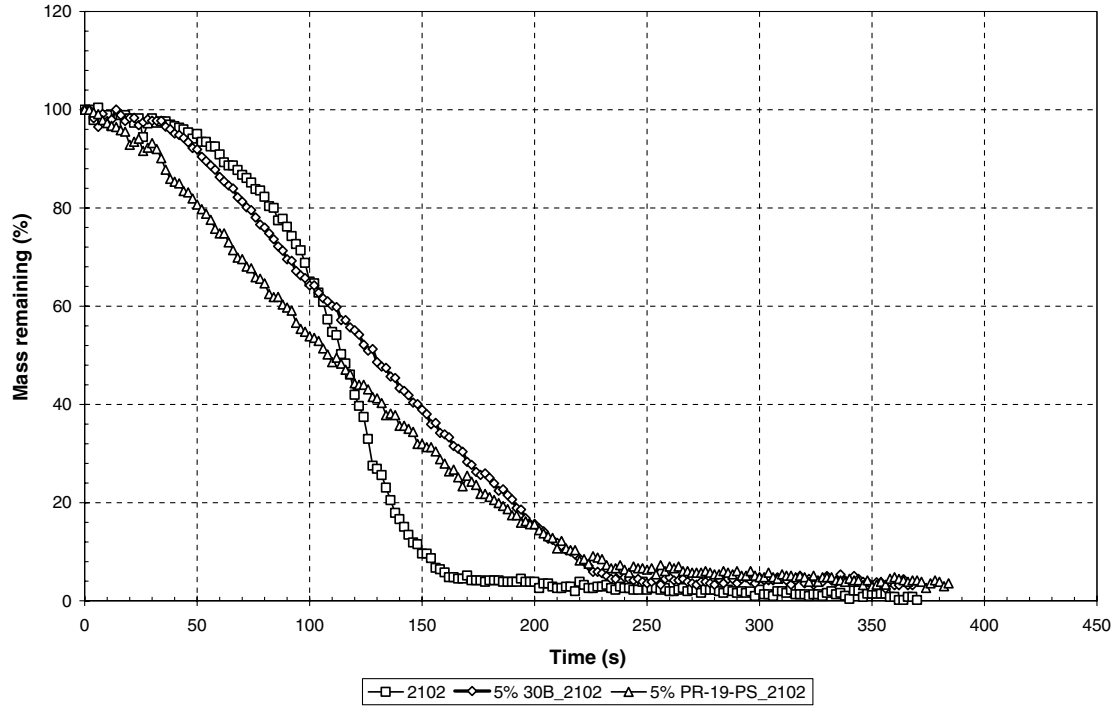

Fig. 25 Mass loss of neat TPU and TPUNs.

release rates (PHRRs) relative to the TPU, with a 73% reduction of PHHR (624 kW/m^2) for the 5% PR-19-PS TPUN material and a 71% reduction of PHHR for the 5% Cloisite 30B TPUN material (644 kW/m^2) as compared with a PHHR of 2290 kW/m^2 for the pure TPU. The TPUNs had a lower average heat release rate (HRR) at 180 s than the TPU and average effective heat of combustion.

Figure 24 shows the heat release rates of the three TPU materials. The 5% PR-19-PS TPUN sample was the only material that had a slight increase of time to sustained ignition and a significant reduction of PHRR compared with the baseline TPU. Figure 25 shows the mass remaining percentages of the materials. Both TPUNs had higher mass loss rates for the initial 150 s and experienced lower mass loss rates than the baseline TPU material after 150 s. Figure 26 shows that the CO concentrations of the TPUNs were significantly lower than the pure TPU. Figure 27 shows the smoke concentration of the three materials. It is obvious that both TPUNs had significantly lower smoke concentrations than the pure TPU. As an aside, the low smoke and CO concentration features also made the TPUNs a very attractive class of fire-retardant polymers that have the potential to be used for commercial markets.

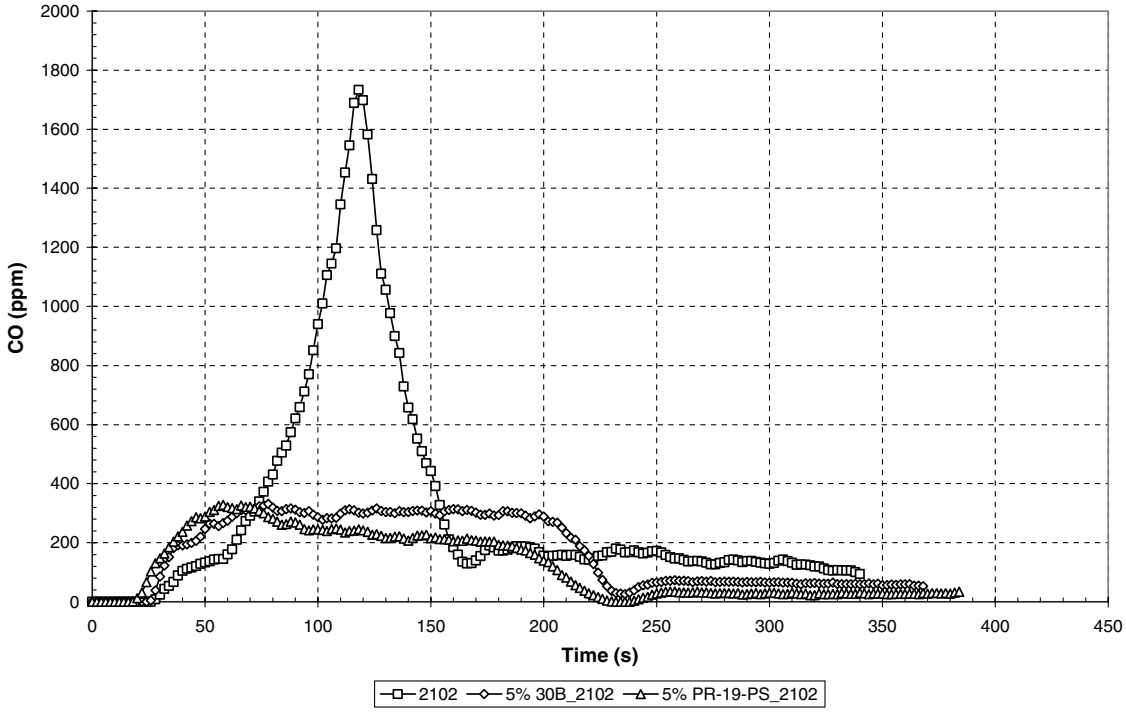

Fig. 26 Carbon monoxide concentration of neat TPU and TPUNs.

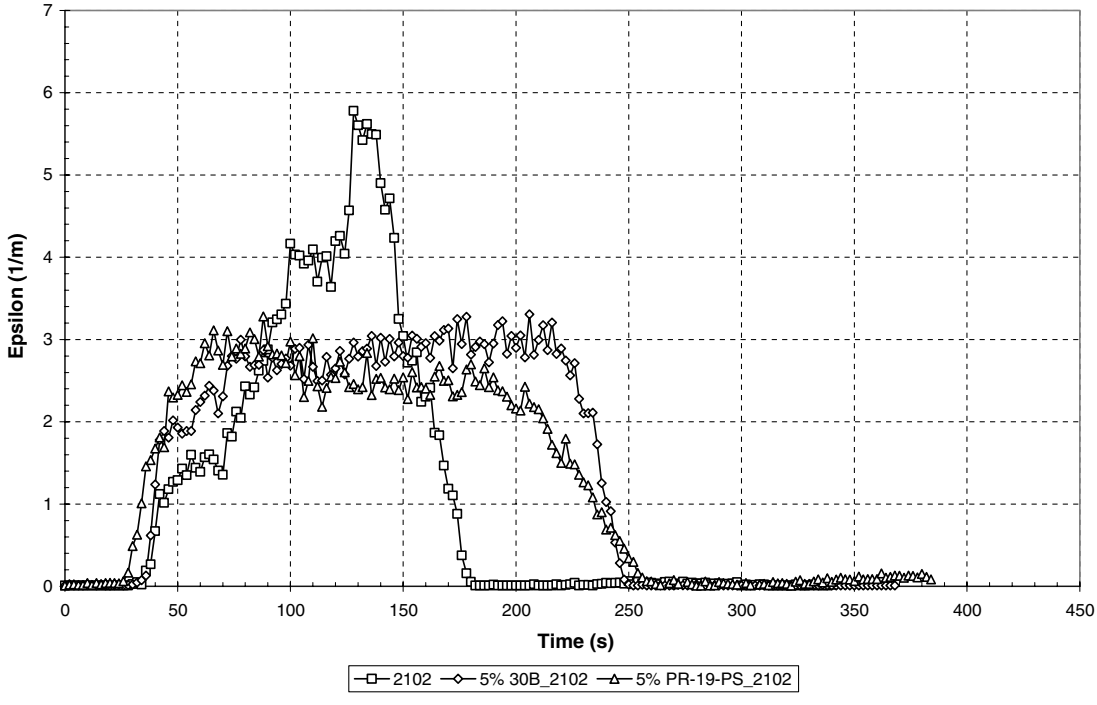

Fig. 27 Smoke concentration of neat TPU and TPUNs.

VI. Conclusions

Formulations of TPU with the addition of 5% Cloisite 30B nanoclay and 15% PR-19-PS carbon nanofibers were blended via twin-screw extrusion. These two formulations ranked highest in their respective family of nanofillers when ablation and mechanical properties were considered and were thus chosen to be the candidates to replace the current state-of-the-art Kevlar-filled EPDM for the next generation of solid rocket motor internal insulation material. TEM and WAXD confirmed that the nanoclays were fully exfoliated in the neat TPU, and TEM showed that the carbon nanofibers were well dispersed in the polymer.

Benchmarking experiments were conducted first to validate the methods in calculating the kinetic parameters using thermogravimetric analyses. The kinetic parameters of MXBE-350 and Plexiglas specimens were compared with data published by Henderson [27] and in the open literature. Dynamic thermogravimetric analyses in nitrogen at six different heating rates were performed to obtain the kinetic parameters for both formulations (TPUN-clay and TPUN-CNF) as well as the baseline Kevlar-filled EPDM and pure TPU. Weight loss and weight-loss rate measurements were recorded. All formulations exhibited expected behavior. As the heating rate was increased, the temperature of weight loss shifted to higher values, delaying the solid conversion. Closed-loop verification showed that both the modified Friedman and isoconversion methods provided reasonably accurate kinetic parameters for the benchmarking materials, but in the calculations for the proposed TPUN formulations, the modified Friedman method sometimes produced negative activation energy and an order of reaction that was clearly unrealistic. The isoconversion method did not encounter such problems, and it was adapted for the kinetics calculations in this study. Values of the apparent activation energy and preexponential factor were obtained.

Physical, thermophysical, and flammability properties characterization were performed, including density, specific heat, thermal diffusivity, thermal conductivity, coefficient of thermal expansion, heat release rate, smoke concentration, and gas generation. The low peak heat release rate, smoke concentration, and CO emission also made the TPUNs a very attractive class of fire-retardant polymers that have the potential to be used for commercial markets. These material properties characterization will provide more insight on the thermal response of the material. Continuation of this work should include the proper method of precharring and tailoring the material for specific heat and thermal diffusivity measurements. Once the thermophysical properties are obtained, they should be extrapolated for even higher temperatures. TGA experiments at high heating rates (up to $1000^{\circ}\mathrm{C}/\mathrm{min}$) on several of our TPUNs are in progress to study the effect of heating rate and nanoparticle loading [39]. Advanced population-based models of thermoplastic degradation using optimization [40] with the TGA data will be employed to determine kinetic parameters [39]. These thermophysical properties should then be used in a numerical model using industry-standard ablation codes such as CMA [45], Hero-2D [46], and Chaleur [47] to predict the material behavior at a higher heat flux that closely simulates the solid rocket motor environments.

Acknowledgments

The authors would like to thank Charles Y. -C. Lee of the U.S. Air Force Office Scientific Research (AFOSR) for supporting this project through grant no. FA9550-06-1-0356. The authors also thank Gerry Wissler of 21st Century Polymers for his assistance in compounding and molding the polymer nanocomposite samples, Rusty Blanski and colleagues at the U.S. Air Force Research Laboratory, Edwards Air Force Base, California, for conducting the thermophysical properties measurements. We also thank Zhiping Luo at Texas A&M University's Microscopy and Imaging Center for conducting the transmission electron microscopy analyses.

References

[1] Ho, D. W. K., Koo, J. H., Lee, J., and Ezekoye, O. A., "Thermophysical Properties Characterization of Thermoplastic Polyurethane Elastomer Nanocomposites," AIAA Paper 2008-5146, July 2008.

[2] Koo, J. H., Ho, D. W. K., and Ezekoye, O. A., "A Review of Numerical and Experimental Characterization of Thermal Protection Materials, Part 1: Numerical Modeling," AIAA Paper 2006-4936, July 2006.

[3] Koo, J. H., Ho, D. W. K., Bruns, M. C., and Ezekoye, O. A., "A Review of Numerical and Experimental Characterization of Thermal Protection Materials, Part 2: Property Characterization," AIAA Paper 2007-2131, Apr. 2007.

[4] Koo, J. H., Ho, D. W. K., Bruns, M. C., and Ezekoye, O. A., "A Review of Numerical and Experimental Characterization of Thermal Protection Materials, Part 3: Experimental Testing," AIAA Paper 2007-5773, July 2007.

[5] Curry, D. M., and Tillian, D. J., "Apollo Thermal Protection System Revisited," *2006 National Space & Missile Materials Symposium* [CD-ROM], General Dynamics Information Technology, Fairfax, VA, June 2006.

[6] Pinnavaia, T. J., and Beall, G. W. (eds.), *Polymer-Clay Nanocomposites*, Wiley, New York, 2000.

[7] Krishnamoorti, R., and Vaia, R. A. (eds.), *Polymer Nanocomposites: Synthesis, Characterization, and Modeling*, ACS Symposium Series 804, American Chemical Society, Washington, D.C., 2001.

[8] Morgan, A. B., and Wilkie, C. A. (eds.), *Flame Retardant Polymer Nanocomposites*, Wiley, New York, 2007.

[9] Koo, J. H., *Polymer Nanocomposites: Processing, Characterization, and Applications*, McGraw–Hill, New York, 2006.

[10] Vaia, R. A., Price, G., Ruth, P. N., Nguyen, H. T., and Lichtenhan, J., "Polymer/Layered Silicate Nanocomposites as High Performance Ablative Materials," *Applied Clay Science*, Vol. 15, Nos. 1–2, 1999, pp. 67–92. doi:10.1016/S0169-1317(99)00013-7

[11] Patton, R. D., Pittman, C. U., Wang, L., Hill, J. R., and Day, A., "Ablation, Mechanical and Thermal Conductivity Properties of Vapor Grown Carbon Fiber/Phenolic Matrix Composites," *Composites, Part A: Applied Science and Manufacturing*, Vol. 33, No. 2, 2002, pp. 243–251. doi:10.1016/S1359-835X(01)00092-6

[12] Koo, J. H., Stretz, H., Bray, A., Weispfenning, J., Luo, Z. P., Blanski, R., and Ruth, P., "Nanostructured Ablatives for Rocket Propulsion System—Recent Progress," AIAA Paper 2003-1769, Apr. 2003.

[13] Koo, J. H., Stretz, H., Weispfenning, J. T., Luo, Z. P., and Wootan, W., "Nanocomposite Rocket Ablative Materials: Processing, Microstructure, and Performance," AIAA Paper 2004-1996, Apr. 2004.

[14] Koo, J. H., and Pilato, L. A., "Thermal Properties and Microstructures of Polymer Nanostructured Materials," *Nanoengineering of Structural, Functional, and Smart Materials*, edited by M. J. Schulz, A. D. Kelkar, and M. J. Sundaresan, CRC Press, Boca Raton, FL, 2006, pp. 409–441.

[15] Koo, J. H., Pilato, L. A., and Wissler, G. E., "Polymer Nanostructured Materials for Propulsion Systems," *Journal of Spacecraft and Rockets*, Vol. 44, No. 6, 2007, pp. 1250–1262. doi:10.2514/1.26295

[16] Donskoi, A. A., *Physico-Chemistry of Elastomer Heat-Shield Materials*, Nova Science, Commack, NY, 1998.

[17] Donskoi, A. A., and Baritko, N. V., "Fillers and Their Modifications for Elastomeric Heat-Shielding Materials of Low Density," *Low Flammability Polymeric Materials*, edited by G. E.Zaikov, and N. A. Khalturinskii, Nova Science, Commack, NY, 1999, pp. 119–162.

[18] Mares, G., and Budrugeac, P., "Thermal and Oxidative Stability of Ethylene-Propylene Rubbers," *Elastomer Technology Handbook*, edited by M. P. Cheremisinoff, CRC Press, Boca Raton, FL, 1993, pp. 461–471.

[19] Glockler, J., "Innovative TPE Solutions in Automotive Weather Seal Applications," *TPE '98: New Opportunities for Thermoplastic Elastomers*, Rapra Technology, Ltd., Paper 13, Shawbury, England, U.K., 1998, pp. 1–7.

[20] Schrooten, R., "Recent Advancements in the Application Developments of Thermoplastic Vulcanisates (TPE-V)," *TPE '98: New Opportunities for Thermoplastic Elastomers*, Rapra Technology, Ltd., Paper 2, Shawbury, England, U.K., 1998, pp. 1–4.

[21] Koo, J. H., *Polymer Nanocomposites: Processing, Characterization, and Applications*, McGraw–Hill, New York, 2006, pp. 10–26.

[22] Tibbetts, G. G., Lake, M. L., Strong, K. L., and Rice, B. P., "A Review of the Fabrication and Properties of Vapor-Grown Carbon Nanofiber/Polymer Composites," *Composites Science and Technology*, Vol. 67, Nos. 7–8, 2007, pp. 1709–1718. doi:10.1016/j.compscitech.2006.06.015

[23] Luo, Z. P., and Koo, J. H., "Quantifying the Dispersion of Mixture Microstructures," *Journal of Microscopy*, Vol. 225, No. 22, 2007, pp. 118–125.

[24] Luo, Z. P., and Koo, J. H., "Determining the Layer Dispersion Degree in Polymer Layered Silicate Nanocomposites by Quantitative Transmission Electron Microscopy," *Polymer*, Vol. 49, No. 7, 2008, pp. 1841–1852.

[25] Luo, Z. P., and Koo, J. H., "Quantitative Electron Microscopy of Carbon Nanofibers/Nanotubes Enhanced Polymer Nanocomposites," *Materials Letters*, Vol. 62, No. 20, 2008, pp. 3493–3496.

[26] Friedman, H. L., "Kinetics of Thermal Degradation of Char-Forming Plastics from Thermogravimetry. Application to a Phenolic Plastic," *Journal of Polymer Science, Part C: Polymer Symposia*, Vol. 6, No. 1, 1965, pp. 183–195.

[27] Henderson, J. B., "An Analytical and Experimental Study of the Pyrolysis of Composite Ablative Materials," Ph.D. Dissertation, Oklahoma State Univ., Stillwater, OK, Dec. 1980.

[28] Ceamano, J., Mastral, J. F., Millera, A., and Aldea, M. E., "Kinetics of Pyrolysis of High Density Polyethylene: Comparison of Isothermal and Dynamic Experiments," *Journal of Analytical and Applied Pyrolysis*, Vol. 65, No. 2, 2002, pp. 93–110. doi:10.1016/S0165-2370(01)00183-8

[29] Day, M., and Budgell, D. R., "Kinetics of the Thermal Degradation of Poly(Phenylene Sulfide)," *Thermochimica Acta*, Vol. 203, No. 1, 1992, pp. 465–474. doi:10.1016/0040-6031(92)85217-J

[30] Ho, D. W. K., Koo, J. H., Lee, J., and Ezekoye, O. A., "Kinetics of Thermal Degradation of Thermoplastic Polyurethane Elastomer Nanocomposites," *2008 International SAMPE Technical Conference* [CD-ROM], Society for the Advancement of Material and Process Engineering, Covina, CA, 2008.

[31] Ferriol, M., Gentilhomme, A., Cochez, M., Oget, N., and Mieloszynski, J. L., "Thermal Degradation of Poly(Methyl Methacrylate) (PMMA): Modeling of DTG and TG Curves," *Polymer Degradation and Stability*, Vol. 79, No. 2, 2003, pp. 271–281. doi:10.1016/S0141-3910(02)00291-4

[32] Gao, Z., Kaneko, T., Hou, D., and Nakada, M., "Kinetics of Thermal Degradation of Poly(Methyl Methacrylate) Studied with the Assistance of the Fractional Conversion at the Maximum Reaction Rate," *Polymer Degradation and Stability*, Vol. 84, No. 3, 2004, pp. 399–403. doi:10.1016/j.polymdegradstab.2003.11.015

[33] Hirata, T., Kashiwagi, T., and Brown, J. E., "Thermal and Oxidative Degradation of Poly(Methyl Methacrylate): Weight Loss," *Macromolecules*, Vol. 18, No. 7, 1985, pp. 1410–1418. doi:10.1021/ma00149a010

[34] Holland, J. E., and Hay, J. N., "The Effect of Polymerization Conditions on the Kinetics and Mechanisms of Thermal Degradation of PMMA," *Polymer Degradation and Stability*, Vol. 77, No. 3, 2002, pp. 435–439. doi:10.1016/S0141-3910(02)00100-3

[35] Kang, B. S., Kim, S. G., and Kim, J. S., "Thermal Degradation of Poly (Methyl Methacrylate) Polymers: Kinetics and Recovery of Monomers Using a Fluidized Bed Reactor," *Journal of Analytical and Applied Pyrolysis*, Vol. 81, No. 1, 2008, pp. 7–13. doi:10.1016/j.jaap.2007.07.001

[36] Kashiwagi, T., Hirata, T., and Brown, J. E., "Thermal and Oxidative Degradation of Poly(Methyl Methacrylate): Molecular Weight," *Macromolecules*, Vol. 18, No. 2, 1985, pp. 131–138. doi:10.1021/ma00144a003

[37] Erickson, K. L., "Application of Low-Heating Rate TGA Results to Hazard Analyses Involving High-Heating Rates," *2008 International SAMPE Symposium and Exhibition* [CD-ROM], Society for the Advancement of Material and Process Engineering, Covina, CA 2008.

[38] Marschall, J., and Oser, H., "Simultaneous Characterization of Mass Loss & Pyrolysis Gas Species During Ablator Thermal Decomposition," SRI International Rept. MP 08-023, Menlo Park, CA, May 2008.

[39] Lee, J. C., Koo, J. H., Lam, C. K., Bruns, M. C., Ezekoye, O. A., and Erickson, K. L., "The Effect of Heating Rate and Nanoparticle Loading on Thermoplastic Polyurethane Elastomer Nanocomposite Kinetics," 41st AIAA Thermophysics Conference (submitted for publication).

[40] Bruns, M. C., Koo, J. H., Ezekoye, O. A., "Population-Based Models of Thermoplastic Degradation: Using Optimization to Determine Model Parameters," *Polymer Degradation and Stability* (to be published).

[41] "Standard Test Method for Heat and Visible Smoke Release Rates for Materials and Products Using an Oxygen Consumption Calorimeter," ASTM International, Standard E1534, Rev. A, Philadelphia, Dec. 2008.

[42] Koo, J. H., *Polymer Nanocomposites: Processing, Characterization, and Applications*, McGraw–Hill, New York, 2006, pp. 221–225.

[43] Chipara, M., Lozano, K., Hernandez, A., and Chipara, M., "TGA Analysis of Polypropylene-Carbon Nanofibers Composites," *Polymer Degradation and Stability*, Vol. 93, No. 4, 2008, pp. 871–876. doi:10.1016/j.polymdegradstab.2008.01.001

[44] Yezzi, C. A., and Moore, B. B., "Characterization of Kevlar®/EPDM Rubbers for Use as Rocket Motor Case Insulators," AIAA Paper 86-1489, 1986.

[45] "User's Manual Aerotherm Charring Material Thermal Response and Ablation Program (CMA87S)," Acurex Corp., Aerotherm Div., Rept. UM-87-13/ATD, Mountain View, CA, Nov. 1987.

[46] "Two-Dimensional Heat Transfer and Erosion Analysis Code (Hero-2D)," ATK Thiokol, Brigham City, UT, Jan. 2006.

[47] Amar, A. J., Blackwell, B. F., and Edwards, J. R., "One-Dimensional Ablation with Pyrolysis Gas Flow Using a Full Newton's Method and Finite Control Procedure," AIAA Paper 2007-4535, 2007.

T. Lin
Associate Editor